The imprinted *Zdbf2* gene finely tunes feeding and growth in neonates

Juliane Glaser[1,4], Julian Iranzo[1], Maud Borensztein[1], Mattia Marinucci[1], Angelica Gualtieri[3], Colin Jouhanneau[2], Aurelie Teissandier[1], Carles Gaston-Massuet[3], and Deborah Bourc'his[1*]

1. Institut Curie, PSL Research University, INSERM, CNRS, Paris 75005, France
2. Institut Curie, PSL Research University, Animal Transgenesis Platform, Paris 75005, France
3. Centre for Endocrinology, William Harvey Research Institute, Barts and the London School of Medicine and Dentistry, Queen Mary University of London, London EC1M 6BQ, UK.
4. Present address: RG Development & Disease, Max Planck Institute for Molecular Genetics, Berlin, Germany

* Correspondence: **deborah.bourchis@curie.fr**

ABSTRACT

Genomic imprinting refers to the mono-allelic and parent-specific expression of a subset of genes. While long recognized for their role in embryonic development, imprinted genes have recently emerged as important modulators of postnatal physiology, notably through hypothalamus-driven functions. Here, using mouse models of loss, gain and parental inversion of expression, we report that the paternally expressed *Zdbf2* gene controls neonatal growth in mice, in a dose-sensitive but parent-of-origin-independent manner. We further found that *Zdbf2*-KO neonates failed to fully activate hypothalamic circuits that stimulate appetite, and suffered milk deprivation and diminished circulating Insulin Growth Factor 1 (IGF-1). Consequently, only half of *Zdbf2*-KO pups survived the first days after birth and those surviving were smaller. This study demonstrates that precise imprinted gene dosage is essential for vital physiological functions at the transition from intra- to extra-uterine life, here the adaptation to oral feeding and optimized body weight gain.

Keywords: Genomic imprinting/ Development/ Growth/ Hypothalamus

INTRODUCTION

Genomic imprinting is the process by which a subset of genes is expressed from only one copy in a manner determined by the parental origin. In mammals, genomic imprinting arises from sex-specific patterning of DNA methylation during gametogenesis, which generates thousands of germline differentially methylated regions (gDMRs) between the oocyte and the spermatozoa. After fertilization, the vast majority of gDMRs are lost during the epigenetic reprogramming that the embryonic genome undergoes (Seah & Messerschmidt, 2017). However, some gDMRs are protected through sequence- and DNA methylation-specific recruitment of the KRAB-associated protein 1 (KAP1) complex (Li *et al*, 2008; Quenneville *et al*, 2011; Takahashi *et al*, 2019) and become fixed as imprinting control regions (ICRs). Roughly 20 ICRs maintain parent-specific DNA methylation throughout life and across all tissues in mouse and human genomes, and control the mono-allelic and parent-of-origin expression of approximately 150 imprinted genes (Schulz *et al*, 2008; Tucci *et al*, 2019).

DNA methylation-based genome-wide screens have led to the conclusion that all life-long ICRs have probably been discovered (Proudhon *et al*, 2012; Xie *et al*, 2012). However, a greater number of regions are subject to less robust forms of imprinted DNA methylation, restricted to early development or persisting in specific cell lineages only. Moreover, imprinted genes are often expressed in a tissue- or stage-specific manner (Proudhon *et al*, 2012; Monteagudo-Sánchez *et al*, 2019), adding to the spatio-temporal complexity of genomic imprinting regulation. Finally, while the vast majority of imprinted genes are conserved between mice and humans, a subset of them have acquired imprinting more recently in a species-specific manner (Bogutz *et al*, 2019). Why is reducing gene dosage important for imprinted genes, why does it occur in a parent-of-origin manner and why is it essential for specific organs in specific species are fundamental questions in mammalian development and physiology.

Imprinted genes have long-recognized roles in development and viability *in utero*, by balancing growth and resource exchanges between the placenta and the fetus. Moreover, it is increasingly clear that imprinted genes also strongly influence postnatal physiology (Peters, 2014). Neonatal growth, feeding behavior, metabolic rate and body temperature are affected by improper dosage of imprinted genes in mouse models and human imprinting disorders (Charalambous *et al*, 2014; Ferrón *et al*, 2011; Leighton *et al*, 1995; Li *et al*, 1999; Plagge *et al*, 2004; Nicholls *et al*, 1989; Buiting, 2010). Imprinting-related postnatal effects are recurrently linked to dysfunction of the hypothalamus (Ivanova & Kelsey, 2011), a key organ for orchestrating whole body homeostasis through a complex network of nuclei that produce and deliver neuropeptides to distinct targets, including the pituitary gland that in turn secretes endocrine hormones such as the growth hormone (GH). Accordingly, the hypothalamus

appears as a privileged site for imprinted gene expression (Gregg *et al*, 2010). A typical illustration of such association is provided by a cluster of hypothalamic genes whose dosage is altered in Prader-Willi syndrome (PWS). PWS children present neurological and behavioral impairments in particular related to feeding, in the context of hypothalamic neuron anomalies (Swaab, 1997; Cassidy & Driscoll, 2009). In mouse models, single inactivation of the PWS-associated *Magel2* gene results in neonatal growth retardation, reduced food intake and altered metabolism (Bischof *et al*, 2007; Kozlov *et al*, 2007; Schaller *et al*, 2010). Fine-tuning hypothalamic inputs is particularly important for adapting to environmental changes, the most dramatic one for mammals being the transition from intra- to extra-uterine life at birth. Early mis-adaptation to postnatal life can have far-reaching consequences on adult health, by increasing the risk of metabolic diseases. It therefore is of the outmost importance to thoroughly document the action of imprinted genes, particularly in hypothalamic functions.

Zdbf2 (*DBF-type zinc finger- containing protein 2*) is a paternally expressed gene with preferential expression in the brain (Kobayashi *et al*, 2009; Greenberg *et al*, 2017). It is one of the last-discovered genes with life-long and tissue-wide imprinted methylation, and conserved imprinting in mice and humans, however its function is not yet resolved (Kobayashi *et al*, 2009; Duffié *et al*, 2014). We previously characterized the complex parental regulation of the *Zdbf2* locus: it is controlled by a maternally methylated gDMR during the first week of embryogenesis, but for the rest of life, it harbors a somatic DMR (sDMR) that is paternally methylated (Proudhon *et al*, 2012; Duffié *et al*, 2014) (Figure1A). The maternal gDMR coincides with a promoter that drives paternal-specific expression of a *Long isoform of Zdbf2* (*Liz*) transcript. In the pluripotent embryo, *Liz* transcription triggers *in cis* DNA methylation at the sDMR, allowing de-repression of the canonical promoter of *Zdbf2,* located ~10kb downstream (Greenberg *et al*, 2017) (Figure1A). In fact, although specifically expressed in the embryo where it undergoes stringent multi-layered transcriptional control (Greenberg *et al*, 2019), *Liz* is dispensable for embryogenesis itself. Its sole function seems to epigenetically program expression of *Zdbf2* later in life: genetic loss-of-function of *Liz* (*Liz*-LOF) prevents methylation of the sDMR, giving rise to mice that cannot activate *Zdbf2* –despite an intact genetic sequence– in the hypothalamus and the pituitary gland and display reduced postnatal growth (Greenberg *et al*, 2017). The cause of this growth phenotype and whether it is directly linked to the function and dosage regulation of *Zdbf2* in the brain cells is unknown.

By generating loss-of-function (LOF) and gain-of-function (GOF) mouse mutants, we show here that ZDBF2 is necessary for optimal growth and survival during the nursing period, by stimulating hypothalamic food circuits immediately at birth. Moreover, our data support that the dose but not the parental origin of *Zdbf2* expression is important for its imprinted mode of

action. Altogether, our study illustrates the critical function and proper dose regulation of *Zdbf2* for adaptation to postnatal life.

113 **RESULTS**
114

115 ***Zdbf2* is expressed in the neuro-endocrine cells of the hypothalamo-pituitary axis.**

116 Besides a C2H2 zinc finger motif, the ZDBF2 protein does not contain any obvious functional
117 domain that could inform its molecular function. To gain insights into the role of *Zdbf2*, we first
118 examined the cellular specificity and temporal dynamics of its expression. Comprehensive
119 datasets of adult tissues expression in mice and human suggested *Zdbf2* expression is
120 prevalent in brain tissues and pituitary gland (biogps in mouse tissues:
121 http://biogps.org/#goto=genereport&id=73884 and GTex in human tissues:
122 https://gtexportal.org/home/gene/ZDBF2). Our data endorse this brain and pituitary-specific
123 expression of *Zdbf2* in adult mice and show the highest level of expression in the hypothalamus
124 (Figure S1A) (Greenberg *et al*, 2017).

125 To resolve the cellular specificity of *Zdbf2* expression, we used a previously described
126 *LacZ* reporter *Zdbf2* gene-trap mouse line (Greenberg *et al*, 2017). X-gal staining of 2 week-
127 old brain sections confirmed the expression of *Zdbf2* in various brain tissues and the high
128 specificity in hypothalamic cells that belonged to the peri- and paraventricular nuclei in the
129 anterior area (Figure 1B), and the arcuate, the dorsomedial and the ventromedial nuclei in the
130 lateral hypothalamic area (Figure 1C). Analysis of publicly available single-cell RNA-
131 sequencing (scRNA-seq) data further defined *Zdbf2* expression to be specific to neuronal cells
132 and absent from non-neuronal cells of the hypothalamus (Figure S1B-C) (Chen et al., 2017).
133 The three hypothalamic clusters where *Zdbf2* was the most highly expressed were both
134 glutamatergic (Glu13 and Glu15) and GABAergic (GABA17) neurons from the arcuate and the
135 periventricular hypothalamic regions (Figure S1B). Interestingly, these nuclei synthesize
136 peptides that stimulate hormone production from the pituitary gland, or that control energy
137 balance –food intake, energy expenditure and body temperature– by directly acting on the
138 brain and/or more distal organs (Saper & Lowell, 2014).

139 *Zdbf2* being also expressed in the pituitary gland (Figure S1A), we hypothesized it
140 could have a role in the hypothalamo-pituitary axis. When we exanimated the pituitary gland
141 by X-gal staining, we found *Zdbf2* to be expressed in the anterior and intermediate lobes of
142 the gland and almost undetectable signal in the posterior lobe (Figures 1D and S1D), a pattern
143 that was confirmed from available scRNA-seq data (Figure S1E) (Cheung et al., 2018). The
144 anterior and intermediate lobes that form the adenohypophysis are responsible for hormone
145 production (Mollard *et al*, 2012). The anterior lobe secretes hormones from five different
146 specialized hormone-producing cells under the control of hypothalamic inputs (growth
147 hormone-GH, adrenocorticotropic hormone-ACTH, thyroid stimulating hormone-TSH,

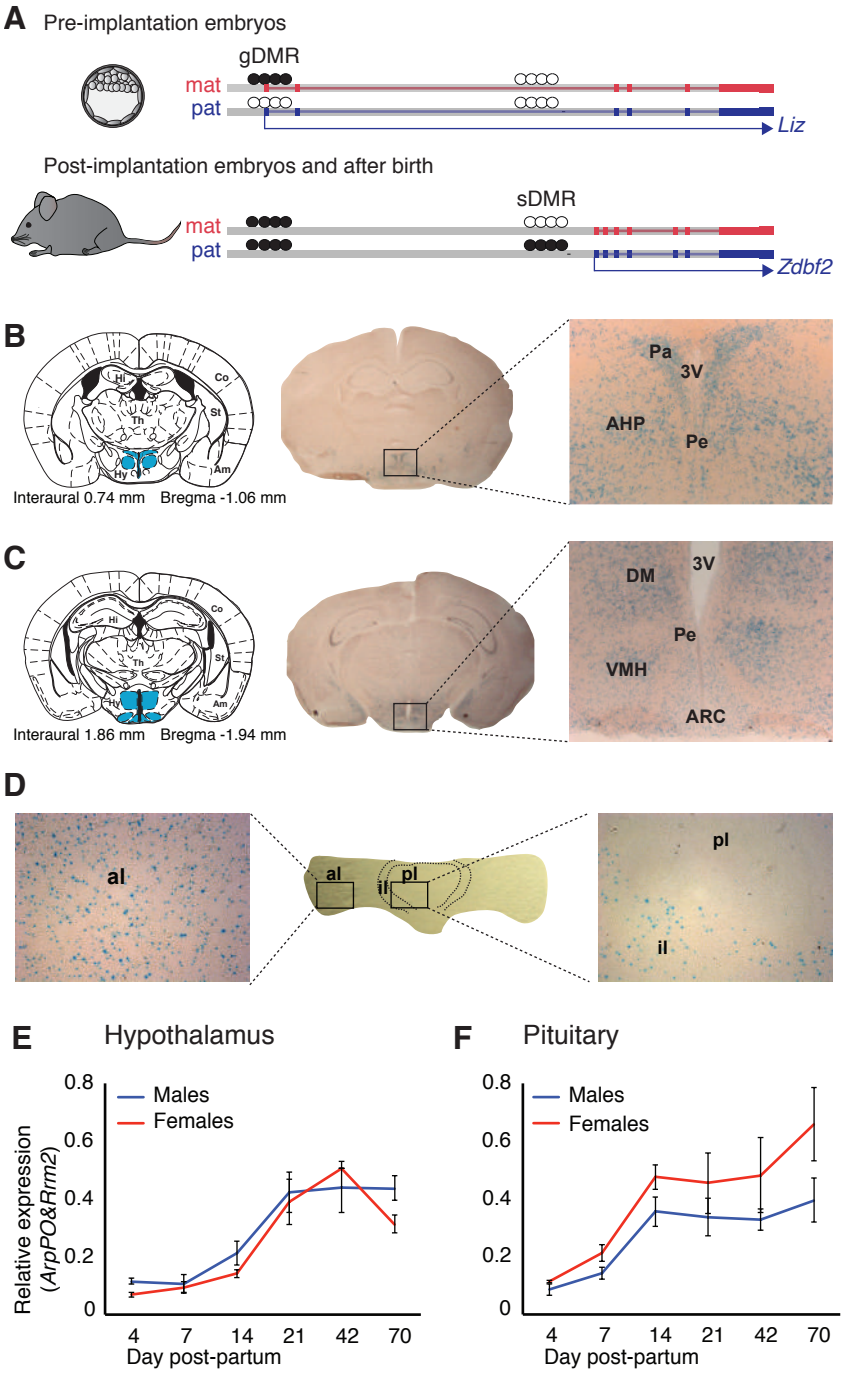

Figure 1: *Zdbf2* expression localizes preferentially in the neuro-endocrine cells of the hypothalamo-pituitary axis in juvenile animals.

(**A**) Scheme of the *Liz/Zdbf2* locus regulation during mouse development. In the pre-implantation embryos, a maternally methylated gDMR allow the paternal-specific expression of the Long isoform of *Zdbf2* (*Liz*). *Liz* expression triggers, in cis, DNA methylation at the sDMR which is localized 8kb upstream of *Zdbf2* canonical promoter. In the post-implantation embryos and for the rest of the life, the imprint at the locus is controlled by the paternal methylation at the sDMR and this allow de-repression of *Zdbf2*, leading to its paternal-specific expression in the post-natal brain. (**B, C**) X-gal staining on brain coronal sections from 2-week-old *Zdbf2*-lacZ transgenic males. The coronal diagram from the Mouse Brain Atlas (left panel) localizes the sections in zone 40 (**B**) and zone 47 (**C**) in stereotaxic coordinates, with the hypothalamus indicated in blue. Whole brain coronal sections (middle panel) show specific staining in the hypothalamus, due to several positive hypothalamic nuclei (right panel, 20X magnificence). Hi, hippocampus; Co, cortex; Th, thalamus; Am, amygdala; St, striatum; Hy, hypothalamus; 3V, third ventricule; Pa, paraventricular hypothalamic nucleus; Pe, periventricular hypothalamic nucleus; AH, anterior hypothalamic area; DM, dorsomedial hypothalamic nucleus; VMH, ventromedial hypothalamic nucleus; Arc, arcuate hypothalamic nucleus. (**D**) X-gal staining on pituitary horizontal sections. The posterior lobe of the pituitary shows no X-gal staining (right panel), while staining is evenly distributed in the anterior lobe (left panel). pl, posterior lobe; il, intermediate lobe; al, anterior lobe. (**E, F**) *Zdbf2* expression measured by RT-qPCR in the hypothalamus (**E**) and the pituitary (**F**) from 4 to 70 days after birth. Data are shown as mean ± s.e.m. of n=3 C57Bl6/J mice.

149 luteinizing hormone-LH and prolactin-PRL) and the intermediate lobe contains
150 melanotrope cells (Kelberman *et al*, 2009). Altogether, the expression specificity of *Zdbf2*
151 suggests a role in functions of the endocrine hypothalamo-pituitary axis and/or of the
152 hypothalamus alone. Finally, we further found that steady-state levels of *Zdbf2* transcripts
153 progressively rose in the hypothalamus and the pituitary gland after birth, reached their
154 maximum at 2-3 weeks and then stabilized at later ages, in both males and females (Figures
155 1E and 1F). The expression of *Zdbf2* therefore mostly increases in juvenile pups prior to
156 weaning.

157

158 **ZDBF2 positively regulates growth postnatally.**

159 In *Liz*-LOF mutants, *Zdbf2* failed to be activated and animals displayed postnatal body weight
160 reduction (Greenberg *et al*, 2017). However, whether this was directly and only linked to *Zdbf2*
161 deficiency was not resolved. To directly probe the biological role of ZDBF2, we therefore
162 generated a mouse model of a genetic loss-of function of *Zdbf2*. More specifically, we
163 engineered a ~700bp deletion of the entirety of exon 6 (Figure 2A) that is common to all
164 annotated *Zdbf2* transcripts (Duffié *et al*, 2014). The *Zdbf2*-Δexon6 deletion induces a frame-
165 shift predicted to generate a severely truncated protein (wild-type 2494aa versus 19aa mutant
166 protein) that notably lacks the zinc finger motif. As *Zdbf2* is an imprinted gene with paternal-
167 specific expression, the deletion should exhibit an effect upon paternal but not maternal
168 transmission. For simplicity, heterozygous mutants with a paternally inherited *Zdbf2*-Δexon6
169 deletion are thus referred to as *Zdbf2*-KO thereafter.

170 At birth, we found that *Zdbf2*-KO animals were present at expected sex and Mendelian
171 ratios (Figures S2A and S2B). However, while exhibiting normal weight prior to birth (at
172 embryonic day E18.5), *Zdbf2*-KO neonates of both sexes failed to thrive from the first day of
173 postnatal life (day post-partum, dpp) (Figure 2B-D). Growth reduction was the most drastic
174 prior to weaning, from 5 to 21dpp (Figure 2B): at 2 weeks of age, *Zdbf2*-KO mice were 20%
175 lighter than their WT littermates (Figures 2B, 2E and 2F). Body weight reduction persisted
176 through adulthood, with a tendency to minimize with age (Figure 2B). As predicted, when
177 present on the maternal allele, the *Zdbf2*-Δexon 6 deletion had no discernable growth effect
178 (Figures S2C and S2D).

179 The reduced body weight phenotype was fully penetrant (Figure S2E) and was not due
180 to a developmental delay: *Zdbf2*-KO pups and their WT littermates synchronously acquired
181 typical hallmarks of postnatal development (skin pigmentation, hair appearance and eye
182 opening) (Figure S2F-I). The growth phenotype appeared to be systemic: it affected both the

183 length and the weight of *Zdbf2*-KO animals (Figure S3A) and all organs uniformly (Figure S3B),
184 such that body proportion was maintained. To gain insight into the origin of the body weight
185 restriction, we performed dual-energy X-ray absorptiometry (DEXA) scan at 7 weeks of age to
186 measure *in vivo* the volume fraction of the three dominant contributors to body composition:
187 adipose, lean, and skeletal tissues (Chen et al., 2012). While we confirmed that adult *Zdbf2*-
188 KO males exhibit an overall body weight reduction (Figure S3C), we did not observe difference
189 in the composition of fat and bone tissues (Figures 2G and S3D-F). However, *Zdbf2*-KO mice
190 had decreased lean mass (Figure 2H). Collectively, the above analyses demonstrate that the
191 product of *Zdbf2* positively regulates body weight gain in juvenile mice.

192 In conclusion, *Zdbf2*-KO animals exhibit the same growth defect that we previously
193 reported in *Liz*-LOF mice, with identical postnatal onset and severity (Greenberg *et al*, 2017).
194 However, contrary to the *Liz*-LOF mice, the regulatory landscape of the paternal allele of *Zdbf2*
195 was intact in *Zdbf2*-KO mice: DNA methylation of the sDMR located upstream of *Zdbf2* was
196 normal (Figure S3G), and accordingly, *Zdbf2* transcription was activated (Figure S3H). This
197 supports that *Liz* transcription in the early embryo —which is required for sDMR DNA
198 methylation (Greenberg *et al*, 2017)— is not impacted in the *Zdbf2*-KO model. We therefore
199 show that a genetic mutation of *Zdbf2* (*Zdbf2*-KO) and a failure to epigenetically program *Zdbf2*
200 expression (*Liz*-LOF) are phenotypically indistinguishable. As *Liz*-LOF mice show a complete
201 lack of *Zdbf2* expression (Greenberg *et al*, 2017), this incidentally supports that *Zdbf2*-KO mice
202 carry a null *Zdbf2* allele. Unfortunately, we failed to specifically detect the mouse ZDBF2
203 protein with commercial or custom-made antibodies.

204

205 ***Zdbf2*-KO neonates fail to thrive or die prematurely within the first week of age.**

206 Growth restriction during the nursing period could dramatically impact the viability of *Zdbf2*-KO
207 pups. Indeed, analysis of *Zdbf2*-KO cohorts revealed that although there was no Mendelian
208 bias at 1dpp (Figure S2B), a strong bias was apparent at 20dpp: 75 WT and 44 *Zdbf2*-KO
209 animals were weaned among *n*=27 litters, while a 50/50 ratio was expected. Post-natal
210 survivability was the most strongly impaired within the first days after birth, with only 56% of
211 *Zdbf2*-KO males and 52% of *Zdbf2*-KO females still alive at 3dpp, compared to 84 and 88% of
212 WT survival at this age (Figure 2I and Supplemental Table 1A). Importantly, a partial postnatal
213 lethality phenotype was also present in *Liz*-LOF mutants who are equally growth-restricted as
214 a result of *Zdbf2* deficiency (Figure S3I), but did not occur when the mutation was transmitted
215 from the silent maternal allele harboring either the *Zdbf2* deletion or the *Liz* deletion (Figure
216 S3J and S3K and Supplemental Table 1C).

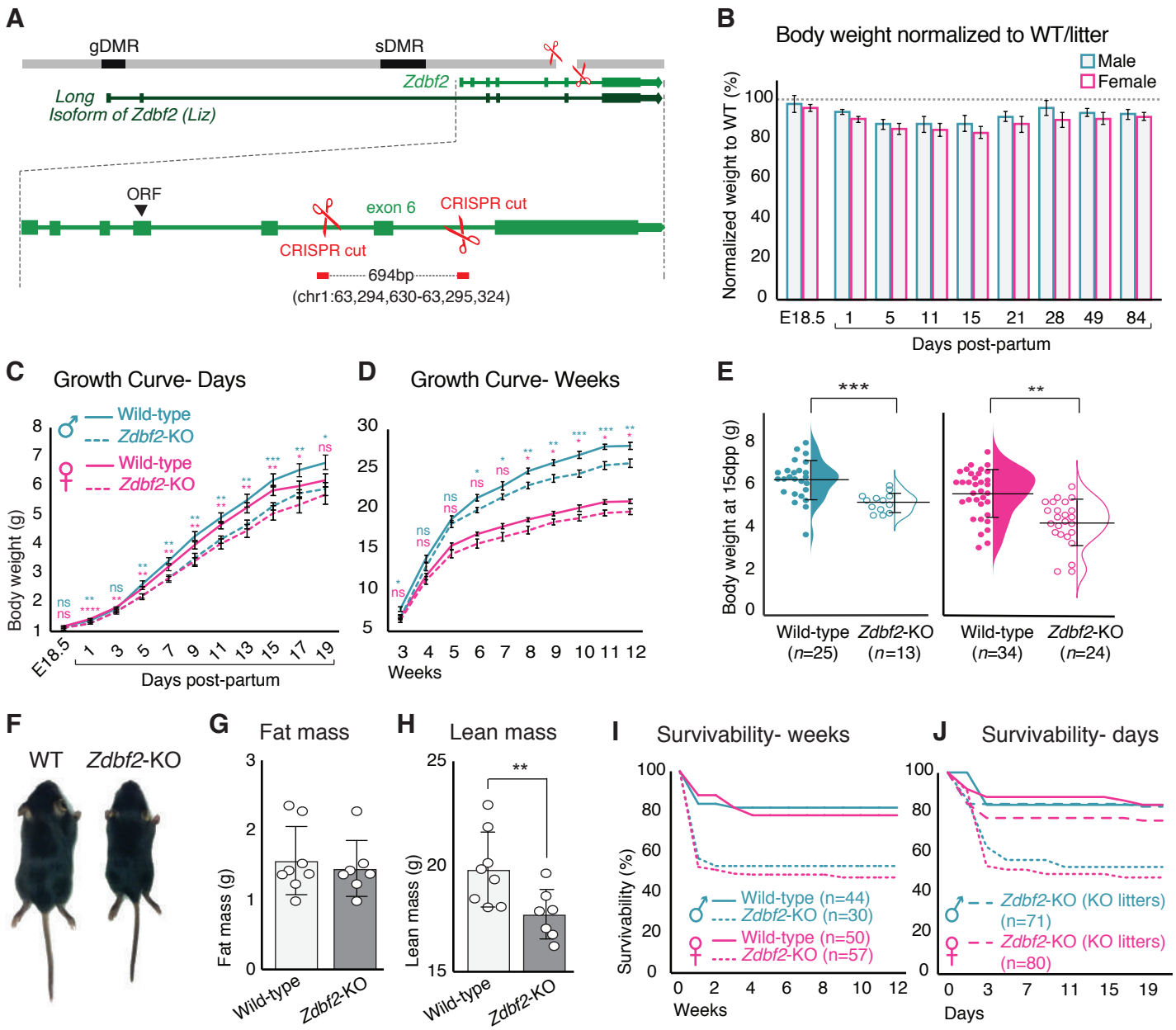

Figure 2: *Zdbf2*-KO mice exhibit growth reduction and partial post-natal lethality.
(**A**) Graphical model of the *Zdbf2* deletion generated using two sgRNAs across exon 6. The two differentially methylated (DMR) regions of the locus are indicated (germline-gDMR, and somatic-sDMR), as well as the Long Isoform of *Zdbf2* (*Liz*). The ORF(Open Reading Frame) of *Zdbf2* starts in exon 4. Genomic coordinates of the deletion are indicated. (**B**) Body weight of *Zdbf2*-KO mice normalized to WT littermates (100%) followed from embryonic day E18.5 to 84 days post-partum. Data are shown as means ± s.e.m. from individuals from n= 27 litters. (**C, D**) Growth curve comparing the body weights of WT and *Zdbf2*-KO mice prior to weaning, from E18.5 to 19dpp (**C**) and over 3 months after birth (**D**). n=15–50 mice were analyzed per genotype, depending on age and sex. Statistical analyses were performed by a two-tailed, unpaired, nonparametric Mann Whitney t test. ***$p \leq 0.001$,**$p \leq 0.01$, *$p \leq 0.05$. (**E**) Half dot plot- half violin plot showing the weight distribution in 2 week-old males (left) and females (right) of WT and *Zdbf2*-KO genotypes. Statistical analyses were performed by a two-tailed, unpaired, nonparametric Mann Whitney t test. ***$p \leq 0.001$,**$p \leq 0.01$, *$p \leq 0.05$. (**F**) Representative photography of a smaller 2 week-old *Zdbf2*-KO male compared to a WT littermate. (**G-H**) Dual-energy X-ray absorptiometry (DXA) analysis showing the calculation of fat mass (**G**) and lean mass (**H**) in WT and *Zdbf2*-KO males at 7 weeks. Data are shown as means ± s.e.m. from n= 8 WT and n=7 *Zdbf2*-KO males. (**I**) Kaplan-Meier curves of the survivability from birth to 12 weeks of age comparing WT (plain lines) and *Zdbf2*-KO (dotted lines) littermates from WT x *Zdbf2* KO/WT backcrosses. Impaired survivability occurs specifically from the first day to 2 weeks of age. (**J**) Kaplan-Meier curves of the survivability from 1 to 21dpp comparing *Zdbf2*-KO pups generated from WT x *Zdbf2* KO/KO intercrosses, with *Zdbf2*-KO and their WT littermates generated from WT x *Zdbf2* KO/WT backcrosses. *Zdbf2*-KO pups are more prone to die only when they are in competition with WT littermates (small dotted lines), while *Zdbf2*-KO pups have a normal survivability when they are not with WT littermates (large dotted lines).

218 To determine whether partial lethality was due to a vital function of ZDBF2, *per se,* or to a
219 competition with WT littermates, we monitored survivability in litters of only *Zdbf2*-KO pups
220 generated from crosses between WT females x homozygous *Zdbf2*-KO/KO males. Litter sizes
221 were similar than the ones sired by *Zdbf2*-KO/WT males. However, when placed in an
222 environment without WT littermates, *Zdbf2*-KO pups gained normal survivability (Figure 2J and
223 Supplemental Table 1B). Incidentally, this shows that *Zdbf2*-KO pups have the mechanical
224 ability to suckle milk. More likely, the impaired survival of *Zdbf2*-KO neonates is a consequence
225 of intra-litter competition with healthier WT pups. Overall, our detailed study of the *Zdbf2*-KO
226 phenotype reveals that smaller *Zdbf2*-KO neonates have reduced fitness compared to their
227 WT littermates. In absence of ZDBF2, after a week of life, half of juvenile pups did not survive
228 and the other half failed to thrive.

229

230 **Postnatal body weight control is highly sensitive to *Zdbf2* dosage**

231 The physiological effects of imprinted genes are intrinsically sensitive to both decreases and
232 increases in the expression of imprinted genes. We therefore went on assessing how postnatal
233 body weight gain responded to varying doses of the imprinted *Zdbf2* gene. We first analyzed
234 the growth phenotype resulting from partial reduction in *Zdbf2* dosage, as compared to a total
235 loss of *Zdbf2* in *Zdbf2*-KO mice. For this, we used the *LacZ* reporter *Zdbf2* gene-trap mouse
236 line (Greenberg *et al*, 2017), in which the insertion of the *LacZ* cassette downstream of exon
237 5 does not fully abrogate the production of full-length *Zdbf2* transcripts (Figure S4A). Upon
238 paternal inheritance of this allele, animals still express 50% of WT full-length *Zdbf2* mRNA
239 levels in the hypothalamus and the pituitary gland (Figure S4B and S4C). Interestingly, these
240 mice displayed significant weight reduction compared to their WT littermates (Figure S4D), but
241 less severe than *Zdbf2*-KO mice (Figure 2B-D). On average, we observed a 5 to 10% weight
242 reduction from 7 to 21dpp, which is incidentally half the growth reduction observed in *Zdbf2*-
243 KO mice for the same age range.

244 We then assessed the consequences of increased *Zdbf2* dosage, with the hypothesis
245 that this would lead to excessive body weight gain after birth, as opposed to reduced *Zdbf2*.
246 For this, we took advantage of a *Zdbf2* gain-of-function (GOF) line that we serendipitously
247 obtained when generating *Liz* mutant mice (Greenberg *et al*, 2017) (see detailed description
248 in Supplemental information). The *Zdbf2*-GOF lines carry a ~ 900bp deletion upstream of *Liz*
249 exon 1, which leaves some part of exon 1 intact and induces an epigenetic "paternalization" of
250 the maternal allele of the locus (Figure S4E and S4F). While sDMR methylation and *Zdbf2*
251 activation exclusively occur on the paternal allele during normal development, animals that
252 maternally inherit this partial deletion also acquire sDMR methylation on the maternal allele

253 (Figures 3A and S4F-H) and activate *Zdbf2* from the maternal allele, although slightly less than
254 from the WT paternal allele (Figure 3B). As a consequence, *Zdbf2*-GOF animals exhibit bi-
255 allelic *Zdbf2* expression, with a net 1.7-fold increase of *Zdbf2* levels in postnatal hypothalamus
256 and pituitary gland, as compared to WT littermates that express *Zdbf2* mono-allelically, from
257 the paternal allele only (Figure 3C).

258 Importantly, we found that increased *Zdbf2* dosage was indeed impactful for postnatal
259 body weight: *Zdbf2*-GOF animals were consistently overweight (Figure 3D-F), and their
260 viability was normal (Figure S5A-C). Although *Zdbf2* was overexpressed in both *Zdbf2*-GOF
261 males and females, the overgrowth phenotype was male-specific, which may imply stimulation
262 of the phenotype by sex hormones, directly or indirectly. Similar to growth restriction observed
263 in *Zdbf2*-KO mutant mice, increased body weight of *Zdbf2*-GOF males was more pronounced
264 during the nursing period (Figure 3D, G and H) and affected all organs uniformly (Figure S5D).
265 From 10 to 20dpp, *Zdbf2*-GOF juvenile males were 10% heavier when normalized to the
266 average WT siblings from the same litter (Figure 3D). At 2 weeks of age, *Zdbf2*-GOF males
267 were visibly bigger than their WT littermates (Figure 3G and 3H), while females displayed
268 standard normal distribution (Figure S5E). Comparatively, progenies from a paternal
269 transmission of the deletion showed a growth progression similar to their WT littermates
270 (Figure S5F and S5G). Overall, these data illustrate the importance of *Zdbf2* for the regulation
271 of postnatal body weight gain at the onset of postnatal life. We therefore demonstrate that the
272 *Zdbf2* imprinted gene encodes a genuine positive regulator of postnatal body weight gain in
273 mice, with highly attuned dose-sensitive effects.

274

275 ***Zdbf2* regulates post-natal growth in a parent-of-origin independent manner.**

276 Imprinted genes with a paternal expression generally tend to enhance prenatal and postnatal
277 growth (Haig, 2000). Consistently, we found that the paternally expressed *Zdbf2* gene
278 promotes postnatal weight gain. Having determined the dosage effect of *Zdbf2*, we next
279 wondered what role plays the paternal origin of *Zdbf2* expression on postnatal body weight.
280 To invert *Zdbf2* parental expression, we intercrossed the *Liz*-LOF and *Zdbf2*-GOF lines, which
281 consist in a maternalization of the paternal allele and a paternalization of the maternal allele of
282 *Zdbf2*, respectively. By crossing an heterozygous *Zdbf2*-GOF female with an heterozygous
283 *Liz*-LOF male (Figure 4A, left panel), four genotypes can segregate in the progeny, with
284 littermates displaying various dosage and parent-of-origin expression of *Zdbf2* (Figure 4A): *1)*
285 wild-type animals with one dose of paternal *Zdbf2* expression, *2)* animals with a paternal *Liz*-
286 LOF allele and lack of *Zdbf2* expression (equivalent to a *Zdbf2*-loss-of-function, *Zdbf2*-LOF),
287 *3)* animals with a maternal *Zdbf2*-GOF allele and biallelic *Zdbf2* expression, and finally, *4)*

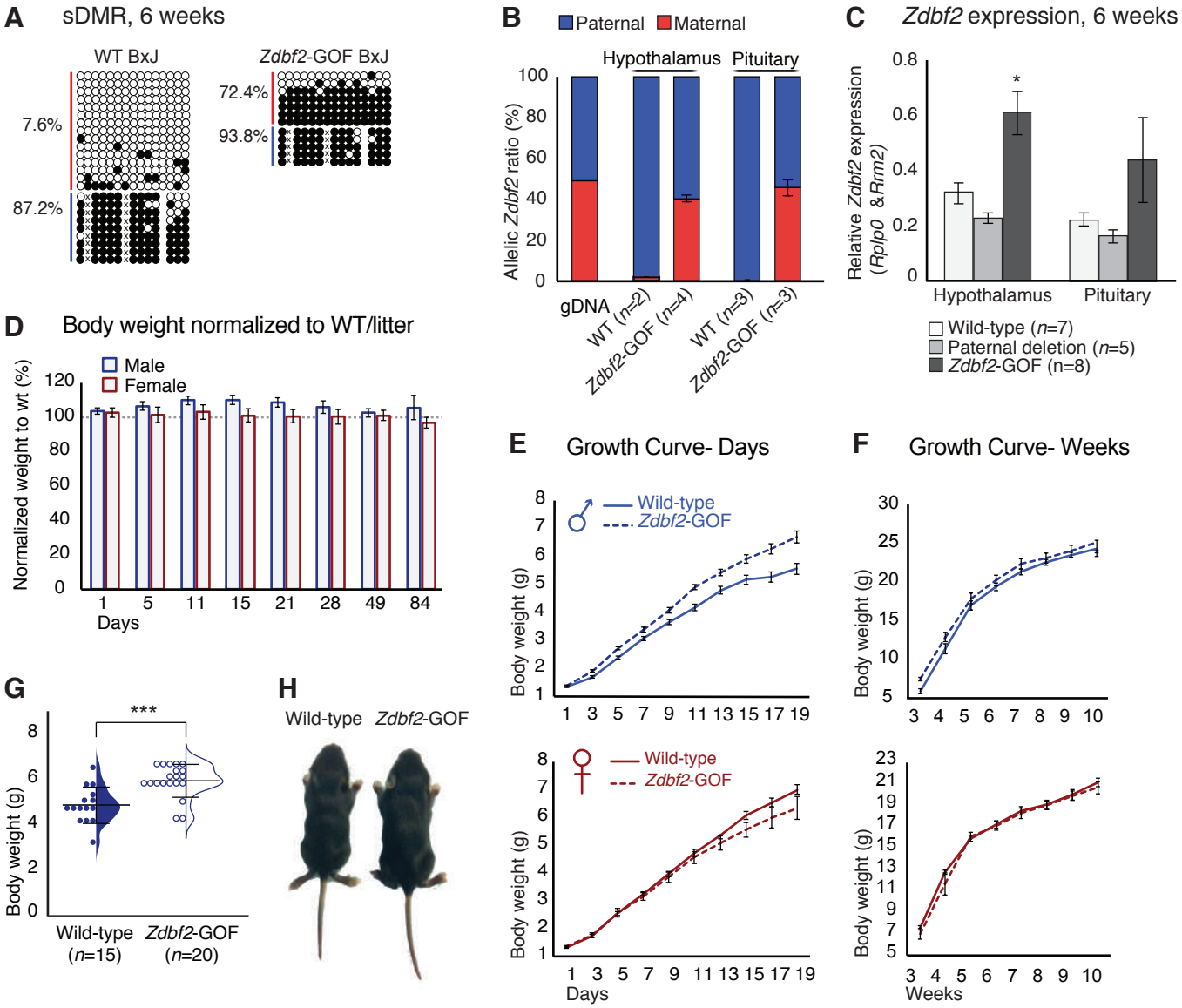

Figure 3: *Zdbf2* influences postnatal growth in a dose-dependent manner.
(**A**) Bisulfite cloning and sequencing showing CpG methylation levels at the sDMR locus of hypothalamus DNA from 6-week-old hybrid WT (left) and *Zdbf2*-GOF (right) mice (*Zdbf2*-GOF +/- x JF1 cross). Red, maternal alleles; blue, paternal alleles. cross, informative JF1 SNP. (**B**) Allelic expression of *Zdbf2* in hypothalamus and pituitary gland from 3-week-old mice, measured by RT-pyrosequencing. Genomic DNA extracted from a C57Bl/6 x JF1 hybrid cross was used as a control for pyrosequencing bias. (**C**) RT-qPCR measurement reveals a ~ 1.7 fold-increase of *Zdbf2* expression in the hypothalamus and pituitary gland of 3 week-old mice with a maternal transmission of the deletion. Expression of *Zdbf2* in mice carrying the deletion on the paternal allele is similar to WT. (**D**) Normalized body growth of *Zdbf2*-GOF mice to their WT littermates (100%) followed at different ages (1 to 84 days) from n=14 litters. The overgrowth is seen specifically in males, from 5 to 28 days. (**E, F**) Growth curves of female and male mice, comparing the body weights of WT and *Zdbf2*-GOF, through the 3 first weeks of life (D) and through 10 weeks (E). n=10–30 mice were analyzed per genotype, depending on age and sex. (**G**) Half dot- half violin plots showing the weight distribution at 2 weeks of age between WT and *Zdbf2*-GOF males. Data are shown as means ± s.e.m. from n individuals. Statistical analyses were performed by a two-tailed, unpaired, nonparametric Mann Whitney t test. *** $p \leq 0.005$. (**H**) Representative photography of a bigger *Zdbf2*-GOF male as compared to a WT littermate at 2 weeks.

289 animals with combined maternal *Zdbf2*-GOF and paternal *Zdbf2*-LOF alleles and potentially,
290 mono-allelic, reverted maternal expression of *Zdbf2* (Figure 4A, right panel).

291 The uniform strain background of the two lines did not allow us to use strain-specific
292 sequence polymorphisms to distinguish the parental origin of *Zdbf2* regulation in the compound
293 *Zdbf2*-GOF/*Zdbf2*-LOF animals. However, we found that compared to single *Zdbf2*-LOF
294 mutants, the presence of the maternal *Zdbf2*-GOF allele restored DNA methylation levels at
295 the sDMR locus in all tissues of *Zdbf2*-GOF/*Zdbf2*-LOF mutants, with an average of 43.5%
296 CpG methylation compared to the expected 50% in WT (Duffié *et al*, 2014) (Figure S5H). By
297 RT-qPCR, *Zdbf2* mRNA levels were also increased in the hypothalamus and pituitary gland of
298 *Zdbf2*-GOF/*Zdbf2*-LOF animals compared to single *Zdbf2*-LOF animals (Figure 4B), which
299 strongly suggests that expression comes from the maternal *Zdbf2*-GOF allele. Accordingly,
300 *Zdbf2* expression level in *Zdbf2*-GOF/*Zdbf2*-LOF animals was on average 0.65-fold the one of
301 WT animals, which is congruent with the partial paternalization of the maternal *Zdbf2*-GOF
302 allele we reported (Figures 4B and S4I). Most importantly, restoration of *Zdbf2* expression by
303 the maternal *Zdbf2*-GOF allele -even though incomplete- was sufficient to rescue the postnatal
304 body weight phenotype in compound *Zdbf2*-GOF/*Zdbf2*-LOF males compared to their single
305 *Zdbf2*-LOF brothers (Figure 4C and 4D). From a body weight reduction of 20% reported in *Liz*-
306 LOF or *Zdbf2*-KO animals at the same age, it was attenuated to only 4% in *Zdbf2*-GOF/*Zdbf2*-
307 LOF animals (Figure 4C), showing that maternal *Zdbf2* expression is as functional as paternal
308 *Zdbf2* expression. Altogether, these results crystallize the importance of *Zdbf2* dosage in
309 regulating postnatal body weight and most importantly, demonstrate that the dose but not the
310 parental origin matters for *Zdbf2* function.

311

312 **_Zdbf2_-KO growth phenotype is linked to decreased IGF-1 in the context of normal**
313 **development of the hypothalamo-pituitary axis.**

314 Having demonstrated the growth promoting effect of *Zdbf2*, we next tackle the question of how
315 it influences newborns weight and survival. As *Zdbf2* is expressed in the neuroendocrine cells
316 of the hypothalamo-pituitary axis, the phenotype of *Zdbf2*-KO animals may lay in a defect in
317 producing growth-stimulating pituitary hormones. When we assessed the development and
318 functionality of the hypothalamus and pituitary gland prior to birth, we did not detect any
319 morphological nor histological defects in *Zdbf2*-KO embryos (Figure S6A-C). Normal
320 expression of major transcriptional regulators confirmed proper cell lineage differentiation in
321 the *Zdbf2*-KO developing pituitary (Figure S6B) (Raetzman *et al*, 2002; Rizzoti, 2015;
322 Kelberman *et al*, 2009). Immunohistochemistry at E18.5 further indicated that *Zdbf2*-KO
323 pituitary cells acquire normal competency for producing hormones (Figure S6D). Similarly,

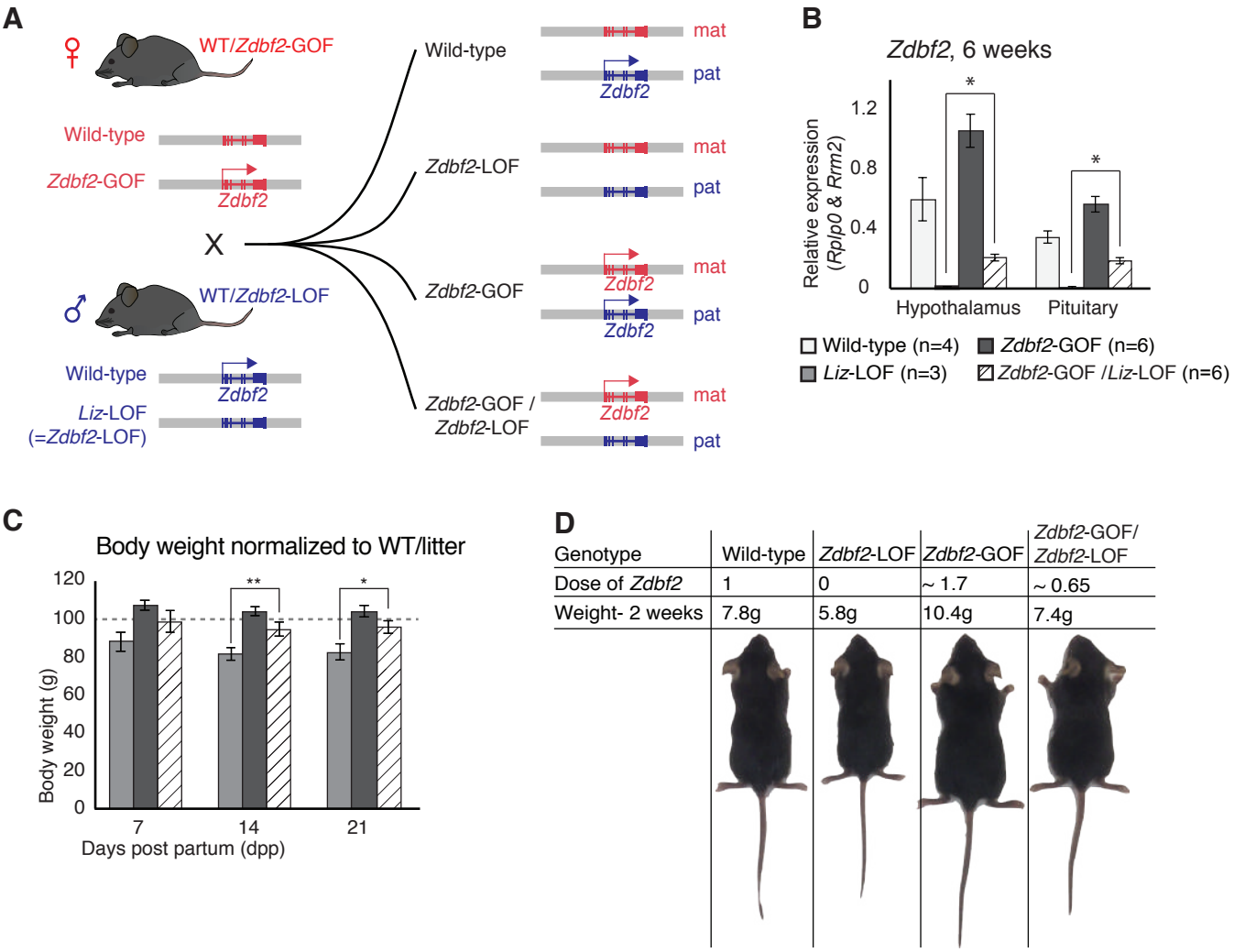

Figure 4: *Zdbf2* influences postnatal growth in a parent-of-origin-independent manner.
(**A**) Scheme of the cross made to obtain embryos with an inversion of the parental origin of *Zdbf2* expression. *Zdbf2*-GOF heterozygote females were crossed with heterozygote males for the *Liz*-LOF deletion- which we demonstrated as equivalent to a *Zdbf2*-LOF allele- (left) to obtain one quarter of embryos expressing one dose of *Zdbf2* from the maternal allele (right, bottom). (**B**) *Zdbf2* expression in the hypothalamus and the pituitary gland is shown in males for each of the four possible genotypes. The level of *Zdbf2* in *Zdbf2*-GOF /*Zdbf2*-LOF mice almost completely rescues the defect seen in *Zdbf2*-LOF and *Zdbf2*-GOF mutants. Data are shown as means ± s.e.m. from n individuals. Statistical analyses were performed by a two-tailed, unpaired, nonparametric Mann Whitney t test. * $p \leq 0.05$. (**C**) Normalized body growth of *Zdbf2*-LOF, *Zdbf2*-GOF and *Zdbf2*-GOF /*Zdbf2*-LOF males to their WT littermates (100%) followed at 7, 14 and 21 days after birth. *Zdbf2*-GOF /*Zdbf2*-LOF adult mice exhibit a body weight similar to the WT showing a partial rescue of the growth reduction and overgrowth phenotype due to respectively the lack of *Zdbf2* and the gain of *Zdbf2* expression in the brain. Data are shown as means ± s.e.m. from individuals from n= 17 litters. Statistical analyses were performed by a two-tailed, unpaired, nonparametric Mann Whitney t test. *$p \leq 0.05$; **$p \leq 0.01$. (**D**) Representative photography of four males littermates from a *Zdbf2*-GOF x *Zdbf2*-LOF cross (as shown in A) at 2 weeks of age. For each animal, genotype, dose of *Zdbf2* expression and weight are indicated.

325 hypothalamic peptides were expressed in comparable levels in *Zdbf2*-KO and WT embryos,
326 as assessed by *in situ* hybridization analysis (Figure S6E and S6F) (Biran *et al*, 2015). In sum,
327 the embryonic hypothalamo-pituitary axis develops normally in the absence of *Zdbf2*. Our data
328 implies that the postnatal growth phenotype does not result from impaired establishment or
329 programming of this axis during embryogenesis.

330 We then went on to analyze the functionality of the hypothalamo-pituitary axis in
331 producing hormones after birth. Again, GH, ACTH, TSH, LH and PRL all appeared to be
332 normally expressed in the pituitary glands of *Zdbf2*-KO juvenile animals
333 (immunohistochemistry at 15dpp) (Figure 5A). Although we cannot exclude subtle
334 dysfunctionalities, our results suggest that *Zdbf2* deficiency does not compromise pituitary
335 hormone production. Hormone release was also functional, as we measured normal plasmatic
336 GH levels in 5 and 15dpp *Zdbf2*-KO animals (Figure 5B). We therefore excluded an
337 involvement of GH in the *Zdbf2*-KO growth phenotype.

338 However, *Zdbf2*-KO pups showed reduced plasma circulating levels of insulin growth
339 factor 1 (IGF-1) –a main marker of postnatal growth– which reached only 50% and 20% of WT
340 level at 5dpp and 15dpp, respectively (Figure 5C). In adult mice, the liver is the main site of
341 production of IGF-1, following transcriptional activation under the control of circulating GH
342 (Savage, 2013). In contrast, extrahepatic production of IGF-1 during embryonic and early
343 postnatal life is mostly GH-insensitive (Lupu *et al*, 2001; Kaplan & Cohen, 2007). As mentioned
344 above, decreased IGF-1 levels in juvenile *Zdbf2*-KO animals indeed occurs in the context of
345 normal GH input. Moreover, we measured normal *Igf1* mRNA levels by RT-qPCR in the liver
346 of juvenile *Zdbf2*-KO animals, further illustrating that decreased IGF-1 levels are not a result
347 of altered GH pathway (Figure 5D).

348 The association of low levels of circulating IGF-1 with normal GH secretion prompted
349 us to evaluate more thoroughly the *Zdbf2*-KO growth phenotype. Mouse models of GH
350 deficiency show growth retardation only from 10dpp onwards, while deficiency in IGF-1 affects
351 growth earlier during postnatal development (Lupu *et al*, 2001). When we calculated the growth
352 rate from day 1 to 8 weeks of age, we revealed two distinct phases: *(1)* from 1 to 7dpp, the
353 *Zdbf2* mutant growth rate was 22% lower compared to WT littermates and *(2)* from 15 to 35dpp,
354 the mutant exceeded the WT growth rate (Figure 5E) (catch up phase), showing that the
355 growth defect is exquisitely restrained to the first days of life. More specifically, at the day of
356 birth (1dpp), *Zdbf2*-KO pups were smaller than their WT littermates by 9% (WT 1.41 $\pm$ 0.015g,
357 n=99; *Zdbf2*-KO 1.29 $\pm$ 0.013, n=95). After 1 week of post-natal life, the mutant growth
358 restriction reached 18% (WT 3.4 $\pm$ 0.13g, n=37; *Zdbf2*-KO 2.8 $\pm$ 0.11, n=17), indicating a failure
359 to thrive prior to 10dpp. Then, at 6 weeks of age, *Zdbf2*-KO animals were smaller than WT by

Glaser et al._ Figure 5

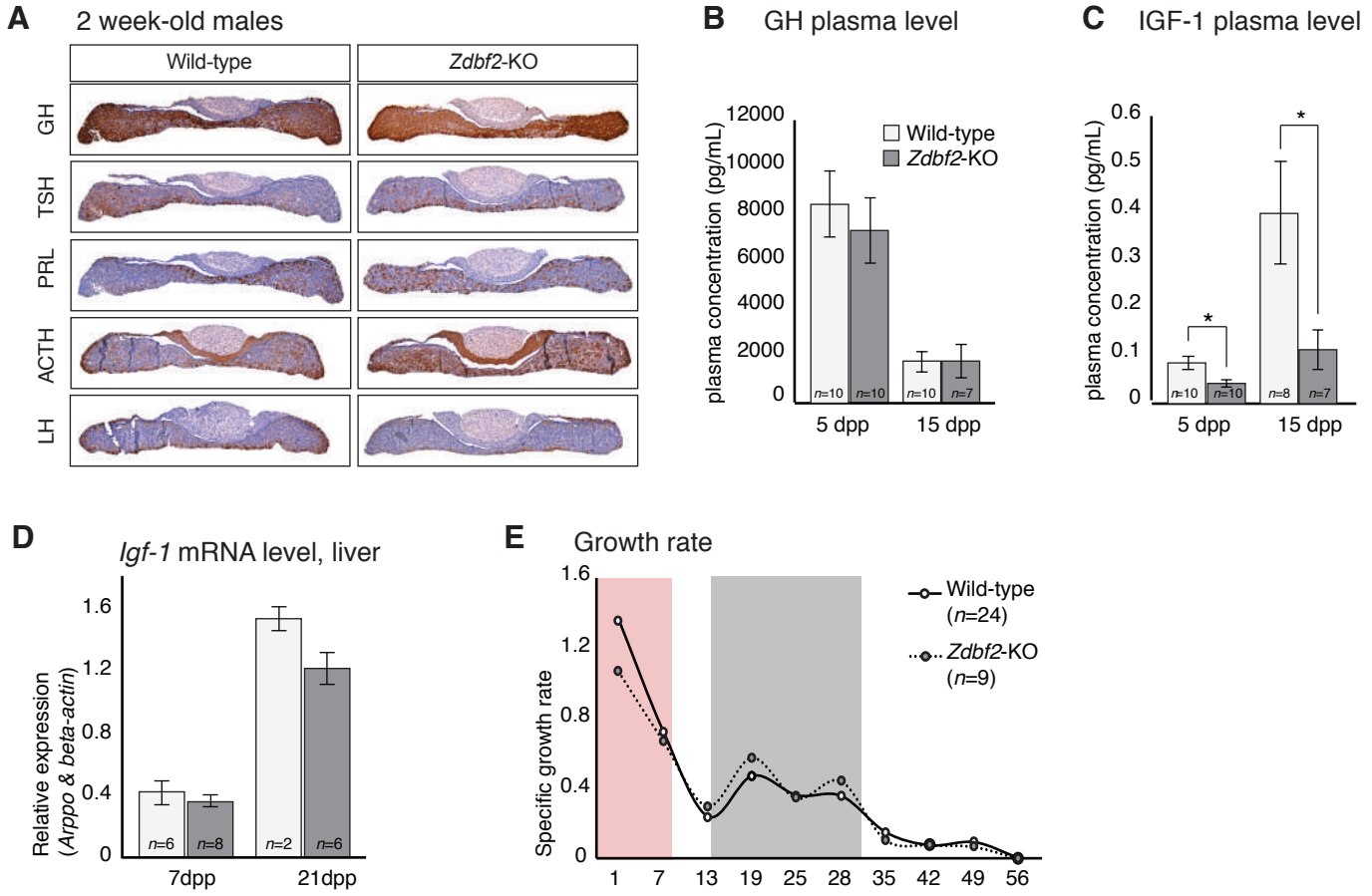

Figure 5: *Zdbf2*-KO phenotype is linked to defective IGF-1 signaling immediately after birth.
(**A**) Pituitary hormone production is globally normal in *Zdbf2*-KO mice, as assessed by immunohistochemistry on 15dpp pituitary sections. (**B, C**) Circulating levels of GH (**B**) and IGF-1 (**C**) in the plasma of WT and *Zdbf2*-KO mice at 5 and 15dpp. Data are shown as means ± s.e.m. from n replicates. Statistical analyses were performed by a two-tailed, unpaired, nonparametric Mann Whitney t test.*$p \leq 0.05$. (**D**) RT-qPCR from post-natal liver measuring the level of *Igf-1* mRNAs between WT and *Zdbf2*-KO mice at 7 and 21dpp. Data are shown as means ±s.e.m from n WT and *Zdbf2*-KO animals. (**E**) Specific growth rates calculated from body weight of WT and *Zdbf2*-KO males from 1 to 56dpp using the following equation: [(weight t2 - weight t1)/ weight t1]. Pink area: reduced growth rate in *Zdbf2*-KO pups compared to WT littermates; Grey area: growth rate of *Zdbf2*-KO mice exceeds the WT growth rate.

361 only 8%, as a result of enhanced post-pubertal growth spurt (WT 21.7 ± 0.04g, *n*=34; *Zdbf2*-
362 KO 20.05 ± 0.3, *n*=15). We therefore concluded that the *Zdbf2*-KO phenotype is similar to
363 defective IGF-1 signaling immediately after birth.

364 Overall, we revealed that the body weight restriction of *Zdbf2*-KO juveniles is
365 associated with a GH-independent decrease of IGF-1 during the first days of postnatal life, in
366 the context of an overall normal development and functionality of the hypothalamo-pituitary
367 axis.

368

369 ***Zdbf2*-KO neonates are undernourished and do not properly activate hypothalamic**
370 **feeding circuits.**

371 Having determined that *Zdbf2*-KO animals exhibit an *Igf-1*-like phenotype, we attempted to
372 define the origin of the GH-independent reduction of IGF-1 levels. Undernutrition is a well-
373 known cause of IGF-1 level reduction, and also of postnatal lethality (Thissen *et al*, 1994),
374 which we observed in *Zdbf2*-KO pups. To investigate the nutritional status of *Zdbf2*-KO
375 neonates, we weighed stomachs at 3dpp, as a measure of milk intake. *Zdbf2*-KO pups
376 exhibited a significant reduction in stomach weight relative to body mass as compared to their
377 WT littermates (Figures 6A and S7A), suggesting that these pups suffer milk deprivation.
378 Comparatively, other organs showed normal relative weight at this age, at the exception of the
379 interscapular brown adipose tissue (BAT), which was also reduced in *Zdbf2*-KO neonates
380 (Figures 6B and S7A). BAT-mediated thermogenesis regulates body heat during the first days
381 after birth (Cannon & Nedergaard, 2004) and improper BAT function can lead to early postnatal
382 death (Charalambous *et al*, 2012). However, despite being smaller, the BAT of *Zdbf2*-KO
383 neonates appeared otherwise functional, showing normal lipid droplet enrichment on
384 histological sections (data not shown) and proper expression of major markers of BAT
385 thermogenic ability (Figure S7B). The BAT size reduction may therefore not reflect altered BAT
386 ontogeny *per se,* but rather the nutritional deprivation of *Zdbf2*-KO neonates.

387 Because the mothers of *Zdbf2*-KO pups are of WT background, the undernutrition
388 phenotype is unlikely due to defective maternal milk supply. Restoration of viability when
389 placed in presence of KO-only littermates (Figure 2K) further indicated that *Zdbf2*-KO pups are
390 competent for suckling. Defective nutrition may therefore rather result from altered feeding
391 motivation of the *Zdbf2*-KO neonates, specifically during the early nursing period. To test this
392 hypothesis, we performed RNA-seq analysis of dissected hypothalami at 3dpp, when the
393 growth phenotype is the most acute (Figure 6C). Only 11 genes were significantly
394 misexpressed in the *Zdbf2*-KO pups relative to their WT littermates (FDR 10%), with a majority

395 being downregulated genes, including *Npy*, which encodes the Neuropeptide Y. In line with
396 our hypothesis, NPY is secreted from neurons of the hypothalamic arcuate nucleus, where
397 *Zdbf2* is expressed and stimulates food intake and promotes gain weight (Mercer *et al*, 2011).
398 Little is known about the determinants of food intake in neonates (Muscatelli & Bouret, 2018),
399 nonetheless, this prompted us to examine the expression levels of other hypothalamic
400 modulators known to influence feeding behavior in adults. Interestingly, *Zdbf2*-KO pups
401 showed a trend towards downregulation of the Agouti-related peptide (*Agrp*)-encoding gene
402 (Figure 6D), which is co-expressed with *Npy* in a sub-population of hypothalamic neurons and
403 convergently stimulate appetite and food seeking (Gropp *et al*, 2005). It is noteworthy that
404 none of the misregulated genes –including positive regulators of feeding– that we observed at
405 3dpp were continuously misregulated in the hypothalamus at 10dpp, when *Zdbf2*-KO pups
406 enter the catch-up phase (Figure S7C and S7D).

407 Together, these results provide key insights into the origin of the *Zdbf2* mutant
408 phenotype: in absence of *Zdbf2,* the hypothalamic circuit of genes that stimulates food intake
409 may not be properly activated at birth. This is associated with reduced milk intake, reduced
410 body weight gain and suboptimal viability of *Zdbf2*-KO neonates when placed in presence of
411 healthier littermates.

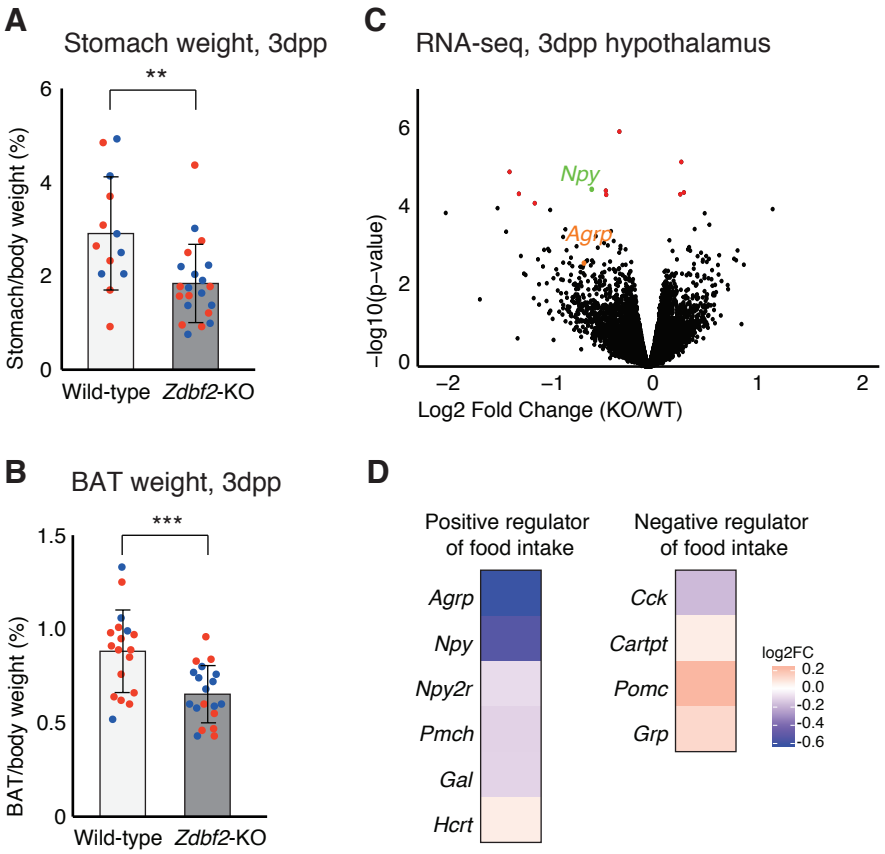

Figure 6: *Zdbf2*-KO neonates display a feeding defect.
(**A, B**) Stomach (**A**) and brown adipocyte tissue (BAT) (**B**) weight normalized to the body weight for WT and *Zdbf2*-KO at 3dpp. Red dots: females; blue dots: males. Data are shown as means ± s.e.m. from n replicates. Statistical analyses were performed by a two-tailed, unpaired, nonparametric Mann Whitney t test.** p≤ 0.01, ***p ≤ 0.005. (**C**) Volcano plot representation of RNA-seq of 3dpp hypothalamus of *Zdbf2*-KO versus WT littermates. Red dots: differentially expressed genes with a threshold of FDR<10%. Npy (FDR 6%) is highlighted in green and Agrp in orange. (**D**) Heatmap showing the log2 fold change of genes encoding hypothalamic regulators of food intake (RNA-seq data from C).

413 **DISCUSSION**

414 The hypothalamus is increasingly regarded as a major site for the action of imprinted genes
415 on postnatal growth, feeding behavior and metabolism (Ivanova & Kelsey, 2011). Here, we
416 found evidence that the imprinted *Zdbf2* gene stimulates hypothalamic feeding circuits, right
417 after birth. In its absence, neonates do not suckle enough milk, and suffer from undernutrition.
418 This leads to decreased IGF-1 signaling within the first week of life, reduced body weight gain
419 and more dramatically, lethality of half of the *Zdbf2*-KO pups when they are in presence of
420 healthier WT littermates. Our work therefore highlights that *Zdbf2* is necessary to thrive and
421 survive after birth, by allowing newborns to adapt to postnatal feeding.

422 By relying on a unique collection of mouse models of total loss of function (*Zdbf2-KO*
423 and *Liz-LOF*), partial loss of function (*Zdbf2*-lacZ), normal function (*Zdbf2*-WT) and gain of
424 function (*Zdbf2*-GOF), we observed that postnatal body growth is exquisitely sensitive to the
425 quantity of *Zdbf2* produced in the hypothalamo-pituitary axis. Incidentally, *Zdbf2* meets the
426 criteria of a *bona fide* growth-promoting gene: growth is reduced upon decreased dosage and
427 oppositely enhanced upon increased dosage of *Zdbf2* (Efstratiadis, 1998). Consistent with
428 previous results for the imprinted *Cdkn1c* gene (Andrews *et al*, 2007), growth reduction was
429 more pronounced than overgrowth upon changes in *Zdbf2* expression (18% decrease and
430 10% increase at 10dpp) and specific to males. This reflects that, with standard diet, overgrowth
431 is a much less frequent response than growth reduction and affects animals with favorable
432 physiology only, potentially explaining male specificity.

433 With a few exceptions, most studies have only addressed the phenotypic effects of
434 reducing the dose of an imprinted gene, but not what results from overexpressing this same
435 gene (Tucci *et al*, 2019). Knocking out an imprinted gene provides valuable insights about its
436 physiological function, however, it does not address the evolutionary significance of imprinting
437 of that gene, *i.e.* reduction to mono-allelic expression. With the *Zdbf2*-GOF model, we were
438 able to evaluate the consequences of a loss of *Zdbf2* imprinting: bi-allelic and increased *Zdbf2*
439 expression exacerbates postnatal body weight gain. However, despite being slightly bigger,
440 viability, fertility or longevity appeared overall normal in *Zdbf2*-GOF animals. The evolutionary
441 importance of *Zdbf2* imprinting is therefore not immediately obvious, at least under
442 unchallenged conditions. Finally, even fewer studies have addressed the importance of parent-
443 of-origin expression for imprinted gene functions (Drake *et al*, 2009; Leighton *et al*, 1995). By
444 intercrossing models of *Zdbf2* loss and gain of function, we could enforce *Zdbf2* expression
445 from the maternal allele while inactivating the normally expressed paternal allele. Restoration
446 of body weight demonstrated the functionality of maternal *Zdbf2* expression, validating that
447 *Zdbf2* functions on postnatal body homeostasis in a dose-dependent but parent-of-origin-

448 independent manner. Although not necessarily surprising, this demonstration is conceptually
449 important for understanding the evolution and *raison d'être* of genomic imprinting. The
450 divergent DNA methylation patterns that are established in the oocyte and the spermatozoa
451 provide opportunities to evolve mono-allelic regulation of expression, but the parental
452 information is not essential *per se*.

453 Although *Zdbf2* is expressed across the hypothalamo-pituitary axis, we could not find
454 evidence of abnormal development or function of the pituitary gland that could explain the
455 *Zdbf2*-KO growth phenotype. Notably, GH production and release was normal. Additionally,
456 the *Zdbf2* growth reduction diverges from GH-related dwarfism: *Gh*-deficient mice grow
457 normally until 10dpp, after which only they exhibit general growth impairment with reduced
458 levels of circulating IGF-1 (Voss & Rosenfeld, 1992; Lupu *et al*, 2001). In *Zdbf2*-KO mutants,
459 the growth defect is apparent as soon as 1dpp and we measured decreased IGF-1 at 5 dpp.
460 In *Igf-1* null mice, birthweight is approximately 60% of normal weight and some mutants die
461 within the first hours after birth (Liu *et al*, 1993; Efstratiadis, 1998). The *Zdbf2*-KO phenotype
462 thus resembles an attenuated *Igf-1* deficiency, in agreement with half reduction but not total
463 lack of circulating IGF-1. Interestingly, similar IGF-1-related growth defects have been reported
464 upon alteration of other imprinted loci: the *Dlk1-Dio3* cluster and the *Cdkn1c* gene (Andrews
465 *et al*, 2007; Charalambous *et al*, 2014). Finally, decreased *ZDBF2* levels have recently been
466 associated with intra-uterine growth restriction (IUGR) in humans (Monteagudo-Sánchez *et al*,
467 2019). Whether this is linked to impaired fetal IGF-1 production would be interesting to assess.

468 IGF-1 secretion has been shown to drop in response to starvation, leading to disturbed
469 growth physiology (Savage, 2013). Our findings support that limited food intake is probably the
470 primary defect in *Zdbf2* deficiency, leading to IGF-I insufficiency in the critical period of
471 postnatal development and consequently, growth restriction. First, we showed that *Zdbf2* is
472 expressed in hypothalamic regions that contain neurons with functions in appetite and food
473 intake regulation, such as the arcuate and paraventricular nucleus. Second, *Zdbf2-KO*
474 neonates show hypothalamic downregulation of the *Npy* and *Agrp* genes that encode for
475 orexigenic neuropeptides (Stanley & Leibowitz, 1984; Ollmann *et al*, 1997). These are likely
476 direct effects, as the rest of the hypothalamic transcriptome is scarcely modified in *Zdbf2*-KO
477 pups. Quantified changes in RNA-seq were not of large magnitude (although significant for
478 *Npy*), but AgRP/NPY neurons represent a very small population of cells, present in the arcuate
479 nucleus of the hypothalamus only (Andermann & Lowell, 2017). We are likely at the limit of
480 detection when analyzing these genes in the whole hypothalamus transcriptome. Finally, *Npy*
481 and *Agrp* downregulation was observed as early as 3 days after birth, along with a phenotype
482 of reduced milk consumption, as measured by stomach weighing. Given our observations, we

483 propose that ZDBF2 activates specialized hypothalamic neurons that motivate neonates to
484 actively demand food (milk) from the mother right at birth, promoting the transition to oral
485 feeding after a period of passive food supply *in utero*. This function agrees with the co-
486 adaptation theory according to which genomic imprinting evolved to coordinate interactions
487 between the offspring and the mother (Wolf & Hager, 2006). Despite considerable effort, we
488 were unable to specifically detect the ZDBF2 protein with antibodies or using epitope-tagging
489 approaches of the endogenous gene; future studies hopefully will bring clarity to which
490 molecular function ZDBF2 carries in the hypothalamus.

491 In conclusion, we reveal here that decreasing *Zdbf2* compromises resource acquisition
492 and body weight gain right after birth. Restricted postnatal growth can have a strong causal
493 effect on metabolic phenotypes, increasing the risk of developing obesity in later life. This is
494 observed in mouse KO models of the imprinted *Magel2* gene that maps to the Prader Willi
495 syndrome region, and in PWS children themselves, who after a failure to thrive as young
496 infants exhibit a catch-up phase leading to overweight and hyperphagia (Bischof *et al*, 2007).
497 *Zdbf2*-KO mice do present a post-puberal spurt of growth, which attenuates their smaller body
498 phenotype, but we never observed excessive weight gain, even after 18 months. It would be
499 interesting to test whether the restricted postnatal growth of *Zdbf2*-KO mice may nonetheless
500 increase the likelihood of metabolic complications when challenged with high-fat or high sugar
501 diet.

502 **MATERIALS AND METHODS**

503 **Mice**

504 Mice were hosted on a 12 h/12 h light/dark cycle with free access to food and water in the
505 pathogen-free Animal Care Facility of the Institut Curie (agreement number: C 75-05-18). All
506 experimentation was approved by the Institut Curie Animal Care and Use Committee and
507 adhered to European and National Regulation for the Protection of Vertebrate Animals used
508 for Experimental and other Scientific Purposes (Directive 86/609 and 2010/63). For tissue and
509 embryo collection, euthanasia was performed by cervical dislocation. The *Zdbf2*-KO and
510 *Zdbf2*-GOF mutant mice lines were derived by CRISPR/Cas9 engineering in one-cell stage
511 embryos as previously described (Greenberg *et al*, 2017), using two deletion-promoting
512 sgRNAs. Zygote injection of the CRISPR/Cas9 system was performed by the Transgenesis
513 Platform of the Institut Curie. Eight week-old superovulated C57BL/6J females were mated to
514 stud males of the same background. Cytoplasmic injection of Cas9 mRNA and sgRNAs (100
515 and 50 ng/ul, respectively) was performed in zygotes collected in M2 medium (Sigma) at E0.5,
516 with well-recognized pronuclei. Injected embryos were cultured in M16 medium (Sigma) at
517 37°C under 5% CO2, until transfer at the 1-cell stage the same day or at the 2-cell stage the
518 following day in the infudibulum of the oviduct of pseudogestant CD1 females at E0.5. The
519 founder mice were then genotyped and two independent founders with the expected deletion
520 were backcrossed to segregate out undesired genetic events, with a systematic breeding
521 scheme of *Zdbf2*-KO heterozygous females x WT C57Bl6/J males and *Zdbf2*-GOF
522 heterozygous males x WT C57Bl6/J females to promote silent passing of the deletion. Cohorts
523 of female and male N3 animals were then mated with WT C57Bl6/J to study the maternal and
524 paternal transmission of the mutation.

525 The LacZ-*Zdbf2* reporter mouse line was derived from mouse embryonic stem (ES)
526 cells from the European Conditional Mouse Mutagenesis Program (EUCOMM Project Number:
527 *Zdbf2*_82543). Proper insertion of the LacZ construct was confirmed by long range PCR.
528 However, upon Sanger sequencing, we found that the loxP site in the middle position was
529 mutated (A to G transition at position 16 of the loxP site) in the original ES cells (Figure S4A).
530 Chimeric mice were generated through blastocyst injection by the Institut Curie Transgenesis
531 platform. We studied animals with an intact LacZ-KI allele, without FRT- or CRE-induced
532 deletions.

533

534 **DNA methylation analyses**

535 Genomic DNA from adult tissues was obtained following overnight lysis at 50°C (100mM Tris
536 pH 8, 5mM EDTA, 200mM NaCl, 0.2% SDS and Proteinase K). DNA was recovered by a
537 standard phenol/choloroform/isoamyl alcohol extraction and resuspended in water. Bisulfite
538 conversion was performed on 0.5-1ug of DNA using the EpiTect Bisulfite Kit (Qiagen). Bisulfite-
539 treated DNA was PCR amplified and either cloned and sequenced, or analyzed by
540 pyrosequencing. For the former, 20-30 clones were Sanger sequenced and analyzed with BiQ
541 Analyzer software (Bock *et al*, 2005). Pyrosequencing was performed on the PyroMark Q24
542 (Qiagen) according to the manufacturer's instructions, and results were analyzed with the
543 associated software.

544

545 **RNA expression analyses**

546 Total RNA was extracted using Trizol (Life Technologies). To generate cDNA, 1ug of Trizol-
547 extracted total RNA was DNase-treated (Ambion), then reverse transcribed with SuperscriptIII
548 (Life Technologies) primed with random hexamers. RT-qPCR was performed using the SYBR
549 Green Master Mix on the ViiA7 Real-Time PCR System (Thermo Fisher Scientific). Relative
550 expression levels were normalized to the geometric mean of the Ct for housekeeping genes
551 *Rrm2*, *B-actin* and/or *Rplp0*, with the ΔΔCt method. Primers used are listed in Supplemental
552 Table 2.

553 For RNA-sequencing, hypothalamus of three animals at 3dpp and two animals at 10dpp were
554 collected for each genotype and RNA was extracted. Trizol-extracted total RNA was DNase-
555 treated with the Qiagen RNase-Free DNase set, quantified using Qubit Fluorometric
556 Quantitation (Thermo Fisher Scientific) and checked for integrity using Tapstation. RNA-seq
557 libraries were cloned using TruSeq Stranded mRNA LT Sample Kit on total RNA (Illumina) and
558 sequencing was performed in 100bp paired-end reads run on a NovaSeq (Illumina) at the
559 NGS platform of the Institut Curie.

560

561 **LacZ staining**

562 Whole brains and pituitary glands were fixed in 4% paraformaldehyde (PFA) in PBS (pH 7.2)
563 overnight and washed in PBS. For sections, tissues were then incubated in sucrose gradients
564 and embedded in OCT for conservation at -80°C before cryosectioning. Sections were first
565 fixed 10 minutes in solution of Glutaraldehyde (0.02% Glutaraldehyde, 2mM MgCl2 in PBS).
566 Tissues and sections were washed in washing solution (2mM MgCl2, 0.02% NP40, 0.01%
567 $C_{24}H_{39}NaO_4$ in PBS) and finally incubated at room temperature overnight in X- gal solution
568 (5mM $K_4Fe(CN)_6 3H_2O$, 5mM $K_3Fe(CN)_6$, 25mg/mL X-gal in wash solution). After several PBS

569 washes, sections were mounted with an aqueous media and conserved at room temperature
570 before imaging.

571

572 **Histological analysis and RNA *in situ* hybridization**

573 Embryos at E13.5 and E15.5 were embedded in paraffin and sectioned at a thickness of 5 µm.
574 For histological analysis, paraffin sections were stained with Haematoxylin and Eosin. RNA *in*
575 *situ* hybridization analysis on paraffin sections was performed following a standard procedure
576 with digoxigenin-labeled antisense riboprobes as previously described (Gaston-Massuet *et al*,
577 2008).The antisense riboprobes used in this study [α-Gsu, *Pomc1*, *Lhx3*, *Pitx1, Avp, oxytocin*
578 *and Ghrh*] have been previously described (Gaston-Massuet *et al*, 2008, 2016).

579

580 **Immunohistochemistry on histological sections**

581 Embryos were fixed in 4% PFA and processed for immuno- detection as previously described
582 (Andoniadou *et al*, 2013). Detection of hormones was carried out using antibodies for α-GH
583 (rabbit polyclonal, NHPP AFP-5641801, 1:1000), α-TSH (rabbit polyclonal, NHPP AFP-
584 1274789, 1:1000), α-PRL (rabbit polyclonal, NHPP AFP-425-10-91, 1:1000), α-ACTH (mouse
585 monoclonal, 10C-CR1096M1, 1:1000) and α-LH (rabbit polyclonal, NHPP AFP-C697071P,
586 1:500).

587

588 **LUMINEX ELISA assay**

589 Plasma from blood was collected in the morning at fixed time on EDTA from 5 and 15 day-
590 old mice after euthanasia and stored at -20C until use. Samples were run in duplicates using
591 the Mouse Magnetic Luminex Assay for IGF-1 (R&D System) and Milliplex Mouse Pituitary
592 Magnetic Assay for GH (Merck) according to manufacturers' instructions. Values were read
593 on Bio-Plex® 200 (Bio-Rad) and analyzed with the Bio-Plex Manager Software.

594

595 **Phenotypic analyses of weight**

596 Postnatal weight measurements were performed every two days from 1dpp to weaning age
597 (21 days). Then, mice were separated according to their genotype, hosted in equal number
598 per cage (n=5 to 6) and weighted once per week. As body weight is a continuous variable, we
599 used a formula derived from the formula for the *t*-test to compute the minimum sample size
600 per genotype: $n=1+C(s/d)^2$, where C is dependent on values chosen for significance level (α)

601 and power (1-β), *s* is the standard deviation and *d* the expected difference in means. Using α
602 =5%, β=90% and an expected difference in means of 1g at 2 weeks and 2g later on, we
603 predicted a minimum *n* of between 10 and 20 and thus decided to increase this number using
604 *n* size between 20 and 30 per genotype, depending of the age and the sex of the mice. No
605 animals were excluded from the analysis. Animals were blindly weighed until genotyping at
606 weaning age. E18.5 embryos and post-natal organs were collected and individually, rinsed in
607 PBS and weighted on a 0.001g scale. All data were generated using three independent mating
608 pairs.

609

610 **Phenotypic analyses of post-natal lethality**

611 Material for genotyping was taken the first day of birth and then number of pups for a given
612 litter was assessed every day. To avoid bias, we excluded from the analysis the litters where
613 all the pups died due to neglecting mothers, not taking care of their pups.

614

615 **DEXA scan analyses**

616 The DEXA analysis allows the assessment of fat and lean mass, bone area, bone mineral
617 content and bone mineral density. Practically, mutant and WT littermate males at 2 weeks
618 were sent from the Animal Facility of Institut Curie to the Mouse Clinics along with their mother
619 (Ilkirch, France). The phenotypic DEXA analysis was performed at 7 weeks of age using an
620 *Ultrafocus DXA* digital radiography system, after the mandatory 5 week-quarantine period in
621 the new animal facility. Mice were anesthetized prior analysis and scarified directly after
622 measurements, without a waking up phase.

623

624 **RNA- seq data analysis**

625 Adapters sequences were trimmed using TrimGalore v0.6.2
626 (https://github.com/FelixKrueger/TrimGalore). Paired-end reads were mapped using
627 STAR_2.6.1a (Dobin *et al*, 2012) allowing 4% of mismatches. Gencode vM13 annotation was
628 used to quantify gene expression using quantification mode from STAR. Normalization and
629 differential gene expression were performed using EdgeR R package (v3.22.3)(Robinson *et*
630 *al*, 2009). Genes were called as differentially expression if the fold discovery rate (FDR) is
631 lower than 10%.

632

633 **Statistical Analyses**

634 Significance of obtained data was determined by performing two-tailed unpaired,
635 nonparametric Mann Whitney *t*- tests using GraphPad Prism6 software. *p* values were
636 considered as significant when $p \leq 0.05$. Data points are denoted by stars based on their
637 significance: **** : $p \leq 0.0001$; *** : $p \leq 0.001$; ** : $p \leq 0.01$; * : $p \leq 0.05$.

638

639 **Data availability**

640 The datasets produced in this study are available in the following databases:
641 RNA-Seq data: Gene Expression Omnibus GSE153265
642 (https://www.ncbi.nlm.nih.gov/geo/query/acc.cgi?acc=GSE153265).

ACKNOWLEDGEMENTS

We would like to thank members of the Bourc'his laboratory for continuous support and stimulation, M. Greenberg for critical reading of the manuscript, M. Charalambous for precious methodological and conceptual advices, T. Chelmicki and L. Marion-Poll for technical help and F. El Marjou (Transgenesis Platform of the Institut Curie Animal Facility) for CRISPR *in vivo* engineering. Luminex assays were performed by the LUMINEX Platform from the CHU Clermont-Ferrand. The laboratory of D.B. is part of the Laboratory d'Excellence LABEX (LABEX) entitled DEEP (11-LBX0044). This research was supported by the ERC (grant ERC-Cog EpiRepro) and the Bettencourt Schueller Foundation. C.G.M. and A.G. were supported by grants from Action Medical Research (GN2272) and BTL Charity (GN417/2238). J.G. was a recipient of PhD fellowships from DIM Biothérapies, Ile-de-France and La Ligue contre le Cancer.

AUTHOR CONTRIBUTION

Conceptualization: D.B. and J.G; Methodology: D.B., J.G. and C.G.M. Formal analysis: J.G. and A.T.; Investigations: J.G., J.I., M.B., M.M., C.J., A.G.; Writing: J.G. and D.B.; Supervision: D.B.; Funding acquisition: D.B. and C.G.M.

COMPETING INTERESTS

The authors declare that they have no competing interests.

663 **REFERENCES**
664

665 Andermann ML & Lowell BB (2017) Toward a Wiring Diagram Understanding of Appetite
666 Control. *Neuron* **95:** 757–778
667 Andoniadou CL, Matsushima D, Mousavy Gharavy SN, Signore M, Mackintosh AI, Schaeffer
668 M, Gaston-Massuet C, Mollard P, Jacques TS, Le Tissier P, Dattani MT, Pevny LH &
669 Martinez-Barbera JP (2013) Sox2+ Stem/Progenitor Cells in the Adult Mouse Pituitary
670 Support Organ Homeostasis and Have Tumor-Inducing Potential. *Cell Stem Cell* **13:**
671 433–445 Available at: https://doi.org/10.1016/j.stem.2013.07.004
672 Andrews SC, Wood MD, Tunster SJ, Barton SC, Surani MA & John RM (2007) Cdkn1c
673 (p57Kip2) is the major regulator of embryonic growth within its imprinted domain on
674 mouse distal chromosome 7. *BMC Dev. Biol.* **7:** 53 Available at:
675 https://pubmed.ncbi.nlm.nih.gov/17517131
676 Biran J, Tahor M, Wircer E & Levkowitz G (2015) Role of developmental factors in
677 hypothalamic function. *Front. Neuroanat.* **9:** 1–11
678 Bischof JM, Stewart CL & Wevrick R (2007) Inactivation of the mouse Magel2 gene results in
679 growth abnormalities similar to Prader-Willi syndrome. *Hum. Mol. Genet.* **16:** 2713–2719
680 Bock C, Reither S, Mikeska T, Paulsen M, Walter J & Lengauer T (2005) BiQ Analyzer:
681 Visualization and quality control for DNA methylation data from bisulfite sequencing.
682 *Bioinformatics* **21:** 4067–4068
683 Bogutz AB, Brind'Amour J, Kobayashi H, Jensen KN, Nakabayashi K, Imai H, Lorincz MC &
684 Lefebvre L (2019) Evolution of imprinting via lineage-specific insertion of retroviral
685 promoters. *Nat. Commun.* **10:** 5674 Available at: https://doi.org/10.1038/s41467-019-
686 13662-9
687 Buiting K (2010) Prader-Willi syndrome and Angelman syndrome. *Am. J. Med. Genet. C.*
688 *Semin. Med. Genet.* **154C:** 365–376
689 Cannon B & Nedergaard J (2004) Brown Adipose Tissue: Function and Physiological
690 Significance. *Physiol. Rev.* **84:** 277–359 Available at:
691 https://doi.org/10.1152/physrev.00015.2003
692 Cassidy SB & Driscoll DJ (2009) Prader–Willi syndrome. *Eur. J. Hum. Genet.* **17:** 3–13
693 Available at: https://doi.org/10.1038/ejhg.2008.165
694 Charalambous M, Ferron SR, Da Rocha ST, Murray AJ, Rowland T, Ito M, Schuster-Gossler
695 K, Hernandez A & Ferguson-Smith AC (2012) Imprinted gene dosage is critical for the
696 transition to independent life. *Cell Metab.* **15:** 209–221
697 Charalambous M, Rocha ST, Hernandez A & Ferguson-smith AC (2014) Perturbations to the
698 IGF1 growth pathway and adult energy homeostasis following disruption of mouse
699 chromosome 12 imprinting. *Acta Physiol* **210:** 174–187
700 Chen R, Wu X, Jiang L & Zhang Y (2017) Single-Cell RNA-Seq Reveals Hypothalamic Cell
701 Diversity. *Cell Rep.* **18:** 3227–3241
702 Chen W, Wilson JL, Khaksari M, Cowley MA & Enriori PJ (2012) Abdominal fat analyzed by
703 DEXA scan reflects visceral body fat and improves the phenotype description and the
704 assessment of metabolic risk in mice. *AJP Endocrinol. Metab.* **303:** E635–E643
705 Cheung LYM, George AS, McGee SR, Daly AZ, Brinkmeier ML, Ellsworth BS & Camper SA
706 (2018) Single-Cell RNA Sequencing Reveals Novel Markers of Male Pituitary Stem
707 Cells and Hormone-Producing Cell Types. *Endocrinology* **159:** 3910–3924
708 Dobin A, Davis CA, Schlesinger F, Drenkow J, Zaleski C, Jha S, Batut P, Chaisson M &
709 Gingeras TR (2012) STAR: ultrafast universal RNA-seq aligner. *Bioinformatics* **29:** 15–
710 21 Available at: https://doi.org/10.1093/bioinformatics/bts635
711 Drake NM, Park JY, Shirali AS, Cleland TA & Soloway PD (2009) Imprint switch mutations at
712 Rasgrf1 support conflict hypothesis of imprinting and define a growth control
713 mechanism upstream of IGF1. *Mamm. Genome* **20:** 654–663
714 Duffié R, Ajjan S, Greenberg M V., Zamudio N, del Arenal Escamilla M, Iranzo J, Okamoto I,
715 Barbaux S, Fauque P & Bourc'his D (2014) The Gpr1/Zdbf2 locus provides new
716 paradigms for transient and dynamic genomic imprinting in mammals. *Genes Dev.* **28:**

717 463–478
718 Efstratiadis A (1998) Genetics of mouse growth. *Int. J. Dev. Biol.* **42:** 955–976
719 Ferrón SR, Charalambous M, Radford E, McEwen K, Wildner H, Hind E, Morante-Redolat
720 JM, Laborda J, Guillemot F, Bauer SR, Fariñas I & Ferguson-Smith AC (2011) Postnatal
721 loss of Dlk1 imprinting in stem cells and niche astrocytes regulates neurogenesis.
722 *Nature* **475:** 381–387
723 Gaston-Massuet C, Andoniadou CL, Signore M, Sajedi E, Bird S, Turner JMA & Martinez-
724 Barbera JP (2008) Genetic interaction between the homeobox transcription factors
725 HESX1 and SIX3 is required for normal pituitary development. *Dev. Biol.* **324:** 322–333
726 Available at: http://www.sciencedirect.com/science/article/pii/S0012160608011196
727 Gaston-Massuet C, McCabe MJ, Scagliotti V, Young RM, Carreno G, Gregory LC, Jayakody
728 SA, Pozzi S, Gualtieri A, Basu B, Koniordou M, Wu C-I, Bancalari RE, Rahikkala E,
729 Veijola R, Lopponen T, Graziola F, Turton J, Signore M, Mousavy Gharavy SN, et al
730 (2016) Transcription factor 7-like 1 is involved in hypothalamo-pituitary axis
731 development in mice and humans. *Proc. Natl. Acad. Sci. U. S. A.* **113:** E548-57
732 Greenberg M, Teissandier A, Walter M, Noordermeer D & Bourc'his D (2019) Dynamic
733 enhancer partitioning instructs activation of a growth-related gene during exit from naïve
734 pluripotency. *Elife* **8:** e44057 Available at: https://doi.org/10.7554/eLife.44057
735 Greenberg MVC, Glaser J, Borsos M, Marjou F El, Walter M, Teissandier A & Bourc'his D
736 (2017) Transient transcription in the early embryo sets an epigenetic state that
737 programs postnatal growth. *Nat. Genet.* **49:** 110–118
738 Gregg C, Zhang J, Weissbourd B, Luo S, Schroth GP, Haig D & Dulac C (2010) High-
739 resolution analysis of parent-of-origin allelic expression in the mouse brain. *Science*
740 **329:** 643–648
741 Gropp E, Shanabrough M, Borok E, Xu AW, Janoschek R, Buch T, Plum L, Balthasar N,
742 Hampel B, Waisman A, Barsh GS, Horvath TL & Brüning JC (2005) Agouti-related
743 peptide–expressing neurons are mandatory for feeding. *Nat. Neurosci.* **8:** 1289–1291
744 Available at: https://doi.org/10.1038/nn1548
745 Haig D (2000) The Kinship Theory of Genomic Imprinting. *Annu. Rev. Ecol. Syst.* **31:** 9–32
746 Available at: https://doi.org/10.1146/annurev.ecolsys.31.1.9
747 Ivanova E & Kelsey G (2011) Imprinted genes and hypothalamic function. *J. Mol. Endocrinol.*
748 **47:**
749 Kaplan SA & Cohen P (2007) REVIEW: The Somatomedin Hypothesis 2007: 50 Years Later.
750 *J. Clin. Endocrinol. Metab.* **92:** 4529–4535 Available at: https://doi.org/10.1210/jc.2007-
751 0526
752 Kelberman D, Rizzoti K, Lovell-Badge R, Robinson ICAF & Dattani MT (2009) Genetic
753 regulation of pituitary gland development in human and mouse. *Endocr. Rev.* **30:** 790–
754 829
755 Kobayashi H, Yamada K, Morita S, Hiura H, Fukuda A, Kagami M, Ogata T, Hata K,
756 Sotomaru Y & Kono T (2009) Identification of the mouse paternally expressed imprinted
757 gene Zdbf2 on chromosome 1 and its imprinted human homolog ZDBF2 on
758 chromosome 2. *Genomics* **93:** 461–472
759 Kozlov S V, Bogenpohl JW, Howell MP, Wevrick R, Panda S, Hogenesch JB, Muglia LJ, Van
760 Gelder RN, Herzog ED & Stewart CL (2007) The imprinted gene Magel2 regulates
761 normal circadian output. *Nat. Genet.* **39:** 1266–1272
762 Leighton PA, Ingram RS, Eggenschwiler J, Efstratiadis A & Tilghman SM (1995) Deletion of
763 the H19 gene region in mice disrupts the imprinting of its neighbouring genes. *Nature*
764 **375:** 34–39
765 Li L-L, Keverne EB, Aparicio SA, Ishino F, Barton SC & Surani MA (1999) Regulation of
766 Maternal Behavior and Offspring Growth by Paternally Expressed Peg3. *Science* **284:**
767 330–334
768 Li X, Ito M, Zhou F, Youngson N, Zuo X, Leder P & Ferguson-Smith AC (2008) A Maternal-
769 Zygotic Effect Gene, Zfp57, Maintains Both Maternal and Paternal Imprints. *Dev. Cell*
770 **15:** 547–557

Liu J-P, Baker J, Perkins AS, Roberteon EJ & Efetratiadis A (1993) Mice carrying null mutations of the genes encoding insulinlike growth factor I (lgt-1) and type 1 IGF receptor (lgf1r). *Cell* **75:** 59–72

Lupu F, Terwilliger J & Lee K (2001) Roles of growth hormone and insulin-like growth factor 1 in mouse postnatal growth. *Dev. Biol.* **229:** 141–162

Mercer RE, Chee MJS & Colmers WF (2011) The role of NPY in hypothalamic mediated food intake. *Front. Neuroendocrinol.* **32:** 398–415 Available at: http://www.sciencedirect.com/science/article/pii/S0091302211000537

Mollard P, Hodson DJ, Lafont C, Rizzoti K & Drouin J (2012) A tridimensional view of pituitary development and function. *Trends Endocrinol. Metab.* **23:** 261–269

Monteagudo-Sánchez A, Sánchez-Delgado M, Mora JRH, Santamaría NT, Gratacós E, Esteller M, de Heredia ML, Nunes V, Choux C, Fauque P, de Nanclares GP, Anton L, Elovitz MA, Iglesias-Platas I & Monk D (2019) Differences in expression rather than methylation at placenta-specific imprinted loci is associated with intrauterine growth restriction. *Clin. Epigenetics* **11:** 35 Available at: https://doi.org/10.1186/s13148-019-0630-4

Muscatelli F & Bouret SGC (2018) Wired for eating: how is an active feeding circuitry established in the postnatal brain? *Curr. Opin. Neurobiol.* **52:** 165–171 Available at: http://www.sciencedirect.com/science/article/pii/S0959438818300862

Nagy TR & Clair AL (2000) Precision and accuracy of dual-energy X-ray absorptiometry for determining in vivo body composition of mice. *Obes. Res.* **8:** 392–398

Nicholls RD, Knoll JHM, Butler MG, Karam S & Lalande M (1989) Genetic imprinting suggested by maternal heterodisomy in non-deletion Prader-Willi syndrome. *Nature* **342:** 281–285 Available at: https://doi.org/10.1038/342281a0

Ollmann MM, Wilson BD, Yang Y-K, Kerns JA, Chen Y, Gantz I & Barsh GS (1997) Antagonism of Central Melanocortin Receptors in Vitro and in Vivo by Agouti-Related Protein. *Science* **278:** 135 LP – 138 Available at: http://science.sciencemag.org/content/278/5335/135.abstract

Peters J (2014) The role of genomic imprinting in biology and disease: An expanding view. *Nat. Rev. Genet.* **15:** 517–530

Plagge A, Gordon E, Dean W, Boiani R, Cinti S, Peters J & Kelsey G (2004) The imprinted signaling protein XLαs is required for postnatal adaptation to feeding. *Nat. Genet.* **36:** 818–826

Proudhon C, Duffié R, Ajjan S, Cowley M, Iranzo J, Carbajosa G, Saadeh H, Holland ML, Oakey RJ, Rakyan VK, Schulz R & Bourc'his D (2012) Protection against De Novo Methylation Is Instrumental in Maintaining Parent-of-Origin Methylation Inherited from the Gametes. *Mol. Cell* **47:** 909–920

Quenneville S, Verde G, Corsinotti A, Kapopoulou A, Jakobsson J, Offner S, Baglivo I, Pedone P V., Grimaldi G, Riccio A & Trono D (2011) In embryonic stem cells, ZFP57/KAP1 recognize a methylated hexanucleotide to affect chromatin and DNA methylation of imprinting control regions. *Mol. Cell* **44:** 361–372

Raetzman LT, Ward R & Camper S a (2002) Lhx4 and Prop1 are required for cell survival and expansion of the pituitary primordia. *Development* **129:** 4229–39

Rizzoti K (2015) Genetic regulation of murine pituitary development. *J. Mol. Endocrinol.* **54:** R55–R73

Robinson MD, McCarthy DJ & Smyth GK (2009) edgeR: a Bioconductor package for differential expression analysis of digital gene expression data. *Bioinformatics* **26:** 139–140 Available at: https://doi.org/10.1093/bioinformatics/btp616

Saper CB & Lowell BB (2014) The hypothalamus. *Curr. Biol.* **24:** R111–R1116

Savage MO (2013) Insulin-Like Growth Factors, Nutrition and Growth. In *World Review of Nutrition and Dietetics* pp 52–59. Available at: https://www.karger.com/DOI/10.1159/000342577

Schaller F, Watrin F, Sturny R, Massacrier A, Szepetowski P & Muscatelli F (2010) A single postnatal injection of oxytocin rescues the lethal feeding behaviour in mouse newborns

825 deficient for the imprinted Magel2 gene. *Hum. Mol. Genet.* **19:** 4895–4905
826 Schulz R, Woodfine K, Menheniott TR, Bourc'his D, Bestor T & Oakey RJ (2008) Wamidex:
827 A web atlas of murine genomic imprinting and differential expression. *Epigenetics* **3:**
828 89–96
829 Seah MKY & Messerschmidt DM (2017) From Germline to Soma: Epigenetic Dynamics in
830 the Mouse Preimplantation Embryo. *Curr. Top. Dev. Biol.* **128:** 203–235
831 Stanley BG & Leibowitz SF (1984) Neuropeptide Y: stimulation of feeding and drinking by
832 injection into the paraventricular nucleus. *Life Sci.* **35:** 2635–2642
833 Swaab DF (1997) Prader-Willi syndrome and the hypothalamus. *Acta Paediatr. Suppl.* **423:**
834 50–54
835 Takahashi N, Coluccio A, Thorball CW, Planet E, Shi H, Offner S, Turelli P, Imbeault M,
836 Ferguson-Smith AC & Trono D (2019) ZNF445 is a primary regulator of genomic
837 imprinting. *Genes Dev.* **33:** 49–54 Available at:
838 https://pubmed.ncbi.nlm.nih.gov/30602440
839 Thissen J-P, Ketelslegers J-M & Underwood LE (1994) Nutritional Regulation of the Insulin-
840 Like Growth Factors*. *Endocr. Rev.* **15:** 80–101
841 Tucci V, Isles AR, Kelsey G, Ferguson-Smith AC, Tucci V, Bartolomei MS, Benvenisty N,
842 Bourc'his D, Charalambous M, Dulac C, Feil R, Glaser J, Huelsmann L, John RM,
843 McNamara GI, Moorwood K, Muscatelli F, Sasaki H, Strassmann BI, Vincenz C, et al
844 (2019) Genomic Imprinting and Physiological Processes in Mammals. *Cell* **176:** 952–
845 965
846 Voss JW & Rosenfeld MG (1992) Anterior pituitary development: Short tales from dwarf
847 mice. *Cell* **70:** 527–530
848 Wolf JB & Hager R (2006) A Maternal–Offspring Coadaptation Theory for the Evolution of
849 Genomic Imprinting. *PLOS Biol.* **4:** e380
850 Xie W, Barr CL, Kim A, Yue F, Lee AY, Eubanks J, Dempster EL & Ren B (2012) Base-
851 resolution analyses of sequence and parent-of-origin dependent DNA methylation in the
852 mouse genome. *Cell* **148:** 816–831
853
854

855 **SUPPLEMENTAL DATA**

856

857 **Generation and characterization of the *Zdbf2*-GOF line**

858 We previously reported the CRISPR/Cas9-mediated generation of *Liz*-LOF mutant mice
859 through targeting a 1.7kb deletion of the entire first exon of *Liz,* including its canonical
860 transcription start site (TSS) (Greenberg et al., 2017). Among the founder mice, some carried
861 a deletion smaller than expected, resulting from non-homologous end joining (NHEJ) repair of
862 the cut induced by the left sgRNA only. Two of these lines –CRISPR-*Liz*_379 and CRISPR-
863 *Liz*_397– exhibited a 924bp and 768bp deletion, respectively, which spanned the region
864 upstream of the *Liz* TSS and left most of the exon 1 of *Liz* intact (Figure S4D). These two lines
865 exhibited an unexpected pattern of DNA methylation at the *Zdbf2* locus upon maternal
866 transmission only: heterozygous embryos at E9.5 with a maternally inherited allele showed a
867 significant gain of sDMR DNA methylation as compared to their WT littermates (Figure S4G).
868 We further demonstrated that the sDMR remained constitutively hypermethylated in adult
869 tissues representative of the three germ layers (Figure S4E).

870 We previously demonstrated that sDMR DNA methylation is positively associated with
871 expression *in cis* of *Zdbf2* in the postnatal hypothalamo-pituitary axis (Greenberg et al., 2017).
872 To decipher if hypermethylation of the sDMR would be able to impact on *Zdbf2* expression,
873 we measured by RT-qPCR the level of *Zdbf2* mRNA in the hypothalamus and the pituitary
874 gland of 3 week-old animals. Focusing on the CRISPR-*Liz*_379 line, we showed increased
875 *Zdbf2* expression upon maternal transmission of the deletion (Figure S4F) and thus named
876 this mutant as *Zdbf2*-gain-of-function (*Zdbf2*-GOF). Allelic analysis from hybrid mice between
877 C57Bl6/J and JF1 strains demonstrated that this gain-of-function was due to ectopic DNA
878 methylation at the sDMR on the maternal allele and ectopic expression of the normally silent
879 maternal *Zdbf2* allele (Figure 3A and B). Reactivation of the maternal allele resulted in bi-
880 allelic, rather than strictly paternal mono-allelic expression of *Zdbf2*. The level of expression of
881 the maternal allele was not equal to the expression of the paternal allele, resulting in a net 1.7-
882 fold increase of *Zdbf2* in *Liz*-GOF animals compared to WT levels (Figure S4F). This was
883 linked to a mosaic gain of DNA methylation on the maternal allele of *Zdbf2*-GOF animals, with
884 70% versus 90-95% of paternal methylation levels. Allelic analysis revealed cellular
885 heterogeneity in the acquisition of methylation of the maternal allele (Figure S4H). In contrast
886 to the effect of the maternal allele, paternal transmission of the deletion behaved as a silent
887 mutation (Figure S4E and F).

888 In sum, we have generated mutant mice with loss-of-imprinting of the *Zdbf2* locus,
889 harboring increased *Zdbf2* dosage in the postnatal brain, as a result of abnormal biallelic
890 expression. The deletion had no effect on the sex and Mendelian distributions upon both

891 maternal and paternal transmission (Figure S5A and B) and the mice survived at the same
892 rate as their WT littermates (Figure S5C). Moreover, we did not detect any fertility or behavioral
893 phenotype in the *Zdbf2*-GOF mice.

Glaser et al._ Supplemental Figure 1

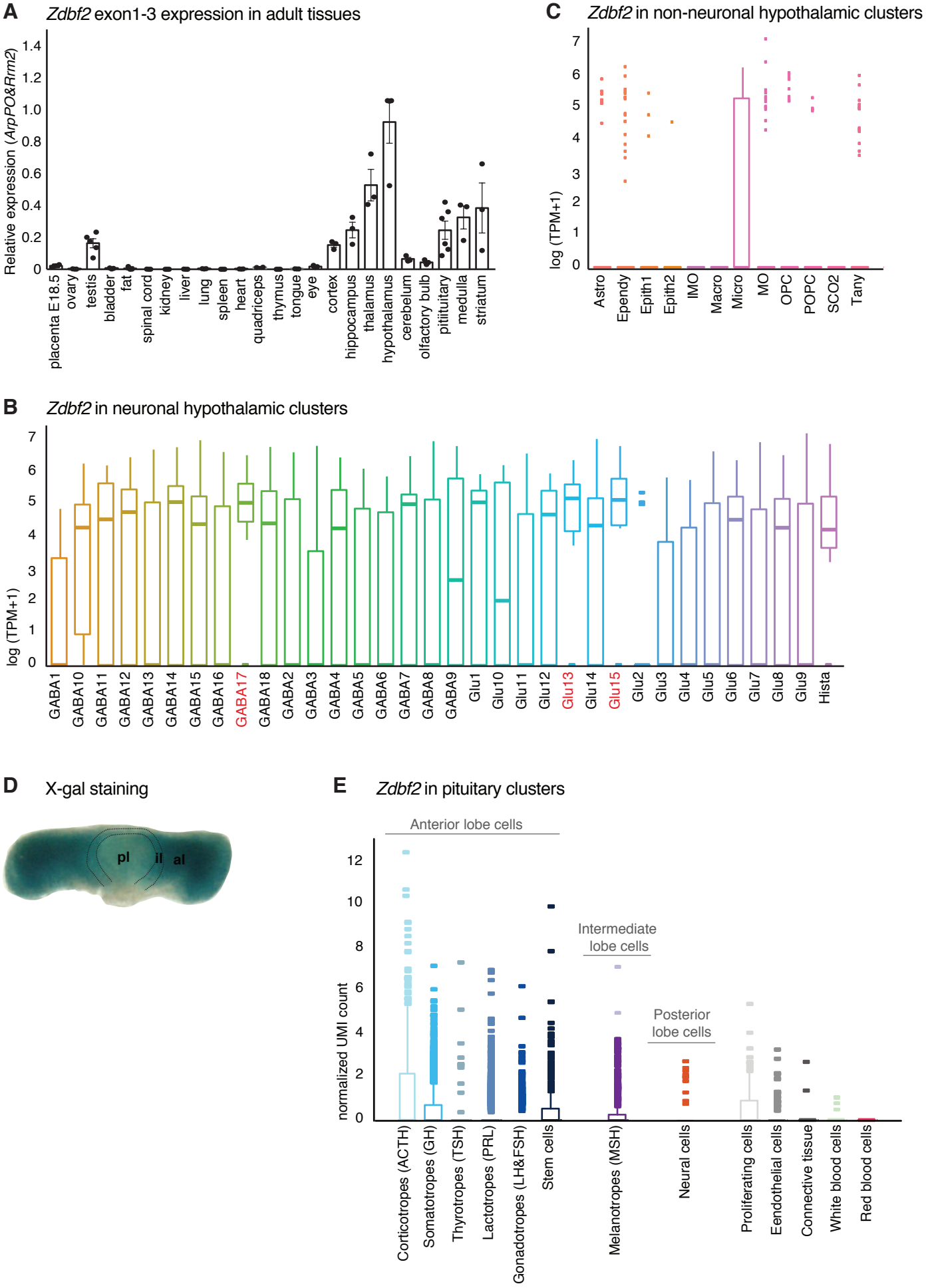

<u>Figure S1</u>: *Zdbf2* expression from pituitary and hypothalamus.
(**A**) Expression of *Zdbf2* measured by RT-qPCR in a bank of adult (6-weeks old) mouse tissues. *Zdbf2* is preferentially expressed in the brain and hypothalamus is the tissue showing the highest level of expression. Data are shown as means ± s.e.m. This figure has been adapted from Greenberg et *al* 2017. (**B, C**) Expression of *Zdbf2* in hypothalamic neuronal (**B**) and non-neuronal (**C**) cell clusters. Clusters where *Zdbf2* expression is the highest are highlighted in red. Single-cell RNA-seq datasets from the hypothalamus of 8 to 10 week-old B6D2F1 females from Chen *et al.*, Cell Reports, 2017. (**D**) Whole-mount pituitary from a *Zdbf2*-LacZ KI mouse stained with X-gal. pl, posterior lobe; il, intermediate lobe; al, anterior lobe. (**E**) Expression of *Zdbf2* in pituitary cell clusters. *Zdbf2* expression is found predominantly in cluster of cells from the anterior and intermediate lobes. Single-cell RNA-seq datasets from pituitaries of 7 week-old C57BL/6J males from Cheung *et al.*, Endocrinology, 2018.

Glaser et al._ Supplemental Figure 2

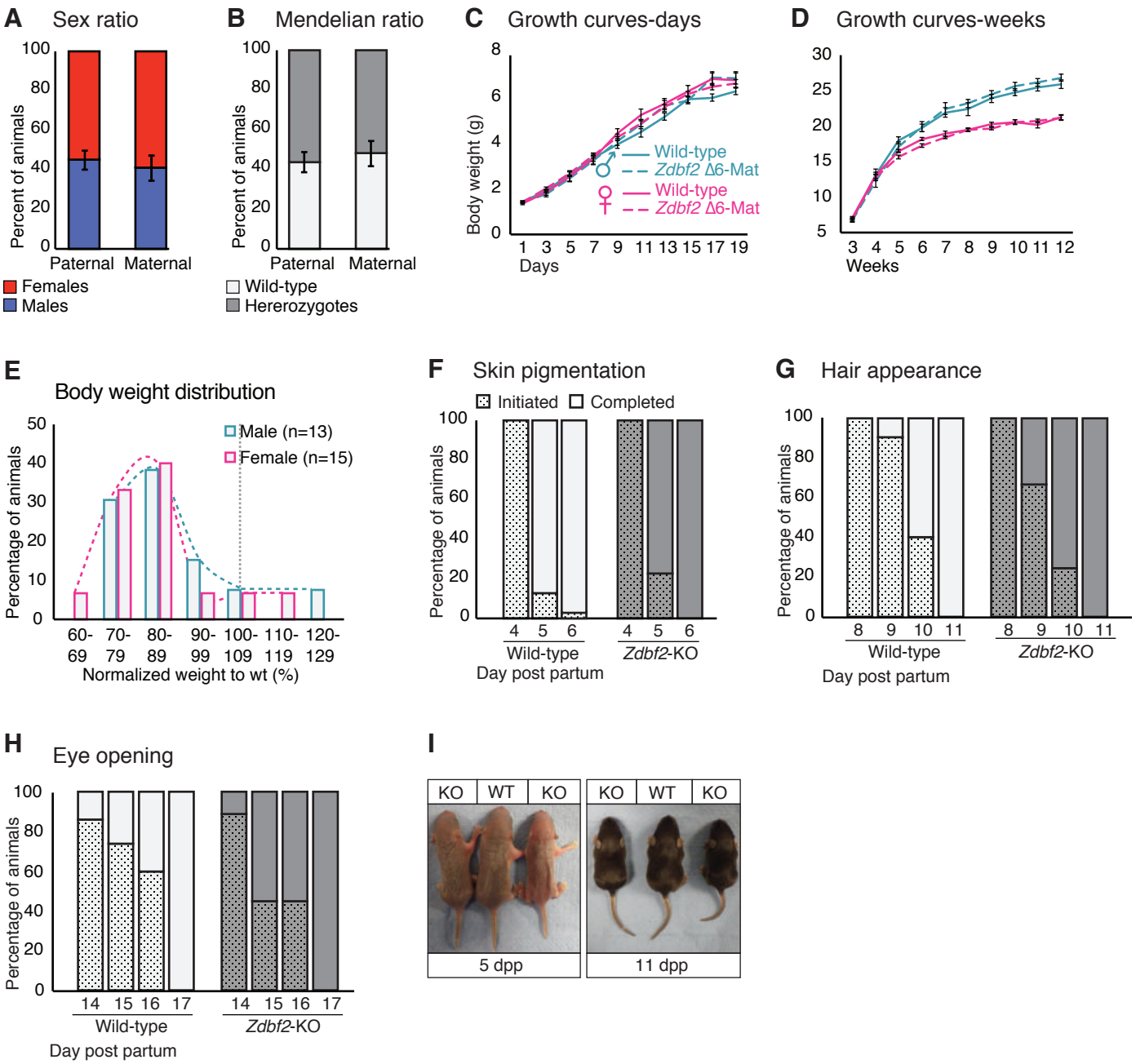

<u>Figure S2</u>: *Zdbf2*-KO pups acquire normal hallmarks of postnatal development.
(**A, B**) Sex ratio (**A**) and genotype ratio (**B**) observed at birth (1dpp) among *Zdbf2* heterozygotes from paternal and maternal transmission of the deletion after three backcrosses. Data are shown as means ± s.e.m. from individuals from n= 32 and 12 litters from paternal and maternal transmission respectively. (**C, D**) Growth curves as in Figure 2C and Figure 2D, respectively, but comparing mutants with a maternal transmission of the Zdbf2 deletion with their WT littermates. (**E**) Frequency of body weight distribution for normalized weights of 2 week-old *Zdbf2*-KO mice relative to WT mice (100%) grouped into 10% bins. The weight reduction phenotype appears to be highly penetrant. (**F-H**) Graphical representation of the timing of three typical hallmarks of postnatal development: skin pigmentation (**F**), hair appearance (**G**) and eye opening (**H**) between WT and *Zdbf2*-KO littermates. (**I**) Representative photography of WT and *Zdbf2*-KO female littermates at 5dpp (left) and 11dpp (right).

Glaser et al._ Supplemental Figure 3

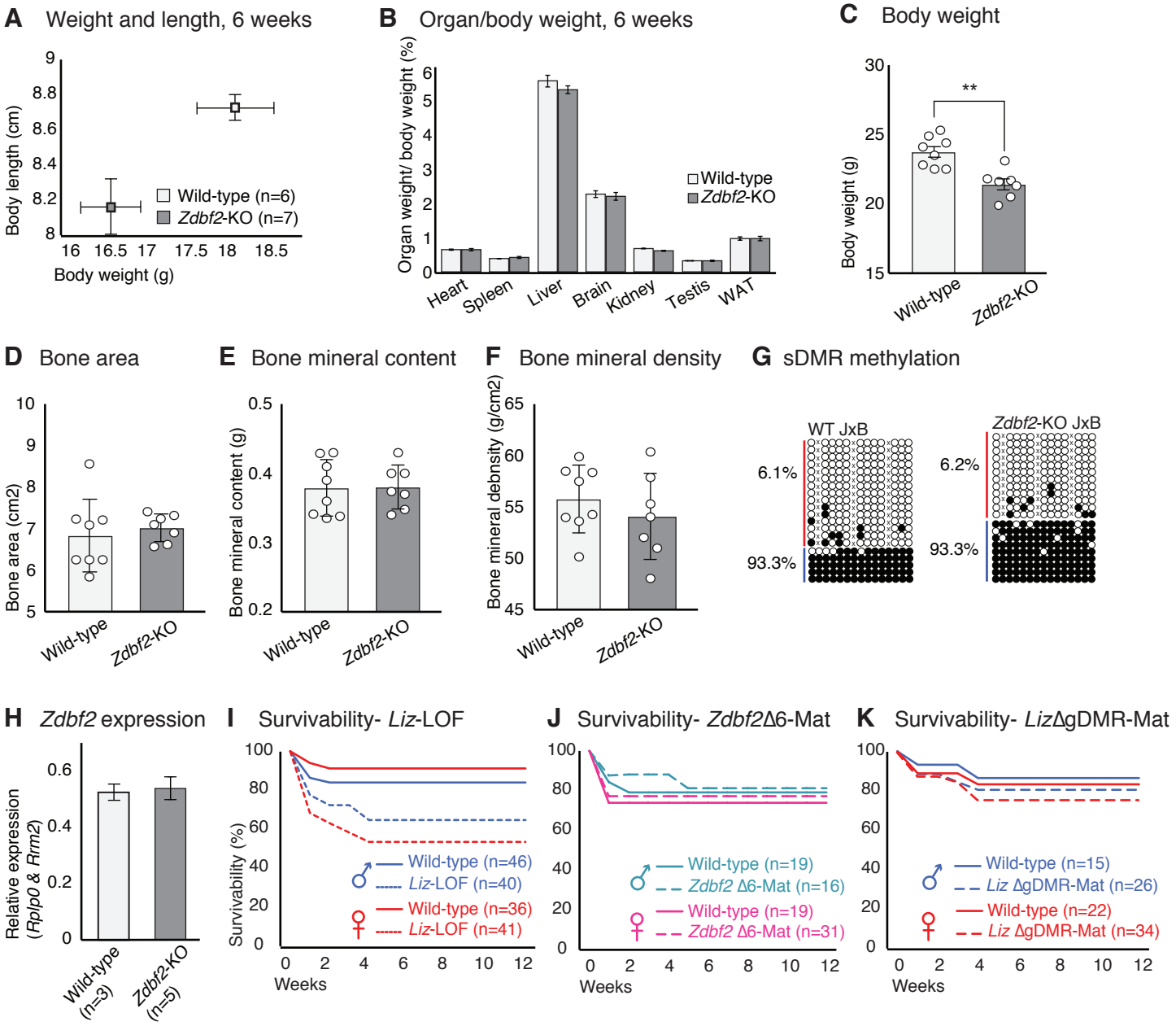

Figure S3: Phenotypic and molecular characterization of *Zdbf2* mutants.
(**A**) Average body length and weight of n WT and *Zdbf2*-KO mice at 6 weeks. (**B**) Individual organ weight plotted as percentage of total body weight in *Zdbf2*-KO mice and WT littermates at 6 weeks.
(**C-F**) Dual-energy X-ray absorptiometry (DXA) showing calculation of body weight (**C**), bone area (**D**), bone mineral content (**E**) and bone mineral density (**F**). Data are shown as means s.e.m from n=8 WT and 7 *Zdbf2*-KO males. (**G**) Bisulfite cloning and sequencing of the sDMR from hypothalamus DNA of 3 week-old hybrid WT (top) and *Zdbf2*-KO (bottom) mice (JF1 x *Zdbf2*-KO cross) reveals that the deposition of DNA methylation at the sDMR is not affected by *Zdbf2* deletion. Red, maternal alleles; blue, paternal alleles. cross, informative JF1 SNP. (**H**) RT-qPCR measuring *Zdbf2* expression from exon 1 to 3 in 3 week-old hypothalamus reveals that *Zdbf2* transcriptional output is not affected by the deletion of the exon 6. Statistical analyses were performed by a two-tailed, unpaired, nonparametric Mann Whitney t test. **p<0.01. (**I-K**) Kaplan-Meier curves of the survivability as in Figure 2I but comparing WT and *Liz*-LOF males and females (**I**), WT and *Zdbf2*-Δexon6 males and females upon maternal transmission of the deletion (**J**) and WT and *Liz*-Δ gDMR males and females upon maternal transmission of the deletion (**K**).

Glaser et al._ Supplemental Figure 4

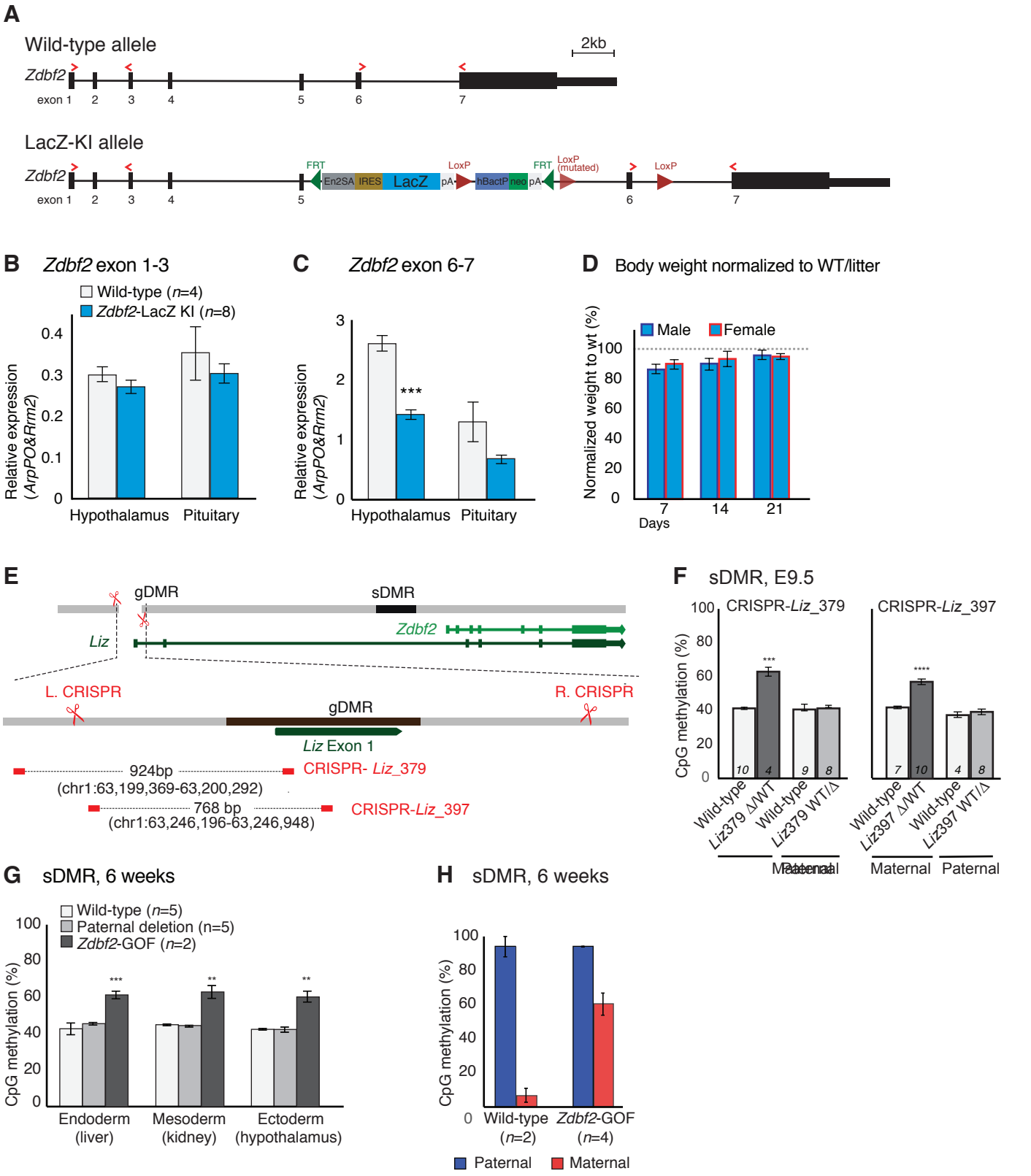

<u>Figure S4</u>: Characterization of partial *Zdbf2*-LOF and *Zdbf2*-GOF mouse lines.
(**A**) Scheme of the wild-type and LacZ-KI *Zdbf2* alleles. The seven exons of the *Zdbf2* transcript are represented by black boxes and the primers used for the RT-qPCR in (**B,C**) are labeled as red arrows. The LacZ-KI allele contains an insertion of: a trapping cassette (En2SA-IRES-LacZ-pA), a Neo cassette under the human beta actin promoter (hbactP-Neo-pA) together with FRT sites to delete the cassettes and LoxP sites to delete exon 6. However, we found the middle loxP site to be non-functional because of a point mutation in the original EUCOMM-provided ES cells. (**B, C**) *Zdbf2* expression measured by RT-qPCR from exon 1-3 (**B**) and exon 6-7 (**C**) in hypothalamus and pituitary of WT and *Zdbf2*-LacZ KI individuals. The insertion schematized in (**A**) leads to a ~ 2-fold decrease in *Zdbf2* expression at exon 6-7, probably due to exon skipping. Data are shown as means ± s.e.m. from n individuals. Statistical analyses were performed by a two-tailed, unpaired, nonparametric Mann Whitney t test. ***$p<0.001$. (**D**) Normalized body growth of *Zdbf2*-LacZ KI mice to their WT littermates (100%) followed at 1, 2 and 3 weeks shows a slight decrease in weight of both males and females. Data are shown as means ± s.e.m. from 8 litters. (**E**) Graphic model of the ΔgDMR CRISPR deletion leading to the generation of the *Liz*_379 founder line (*Zdbf2*-GOF). Deletion is the results of a single cut by Cas9 at the left sgRNA position, followed by NHEJ. (**F**) Bisulfite-pyrosequencing from post-implantation embryos at E9.5 shows increase of sDMR CpG methylation only upon maternal transmission of the deletion, both in *Liz*_379 (left) and *Liz*_397 (right) CRISPR lines. (**G**) Bisulfite-pyrosequencing shows increased sDMR methylation in tissues from 6 week-old mice when the deletion is maternally transmitted. The paternal transmission of the deletion behaves as silent. (**H**) Quantification of allelic sDMR CpG methylation measured by bisulfite cloning and sequencing from n WT and *Zdbf2*-GOF adult tissues. The gain of sDMR methylation from the maternal allele in the mutant compared to their WT littermates is about 65%.

Glaser et al._ Supplemental Figure 5

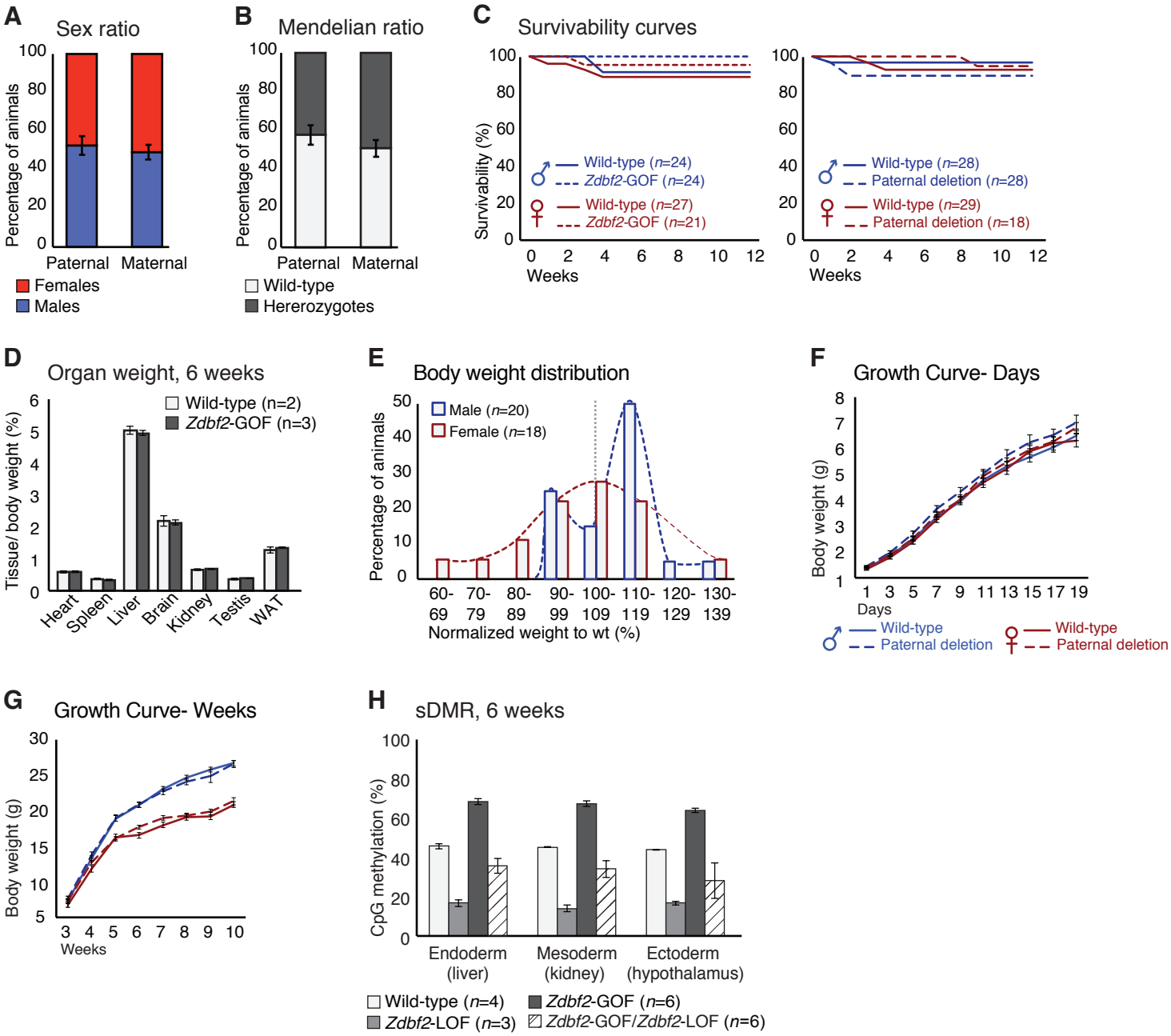

Figure S5: Phenotypic characterization of *Zdbf2*-GOF mutants.
(**A, B**) Sex ratio (**A**) and genotype ratio (**B**) observed at birth among heterozygotes upon paternal and maternal transmission of the *Zdbf2*-GOF mutation after three backcrosses of the *Liz*_379 line. Data are shown as means ± s.e.m. from individuals from n= 15 and 20 litters from paternal and maternal transmission respectively. (**C**) Kaplan-Meier curves of the survivability from birth to 12 weeks showing no lethality phenotype upon maternal (left) and paternal (right) transmission of the deletion, both in males and females. Data are shown as means ± s.e.m. from n individuals. (**D**) Individual organ weight plotted as percentage of total body weight in *Zdbf2*-GOF mice and WT littermates at 6 weeks. (**E**) Frequency of weight distribution for normalized weights of 2-week-old *Zdbf2*-GOF mice relative to WT mice (100%) grouped into 10% bins. The male specific overgrowth phenotype appears to be penetrant. Females show a normal distribution of weight, confirming the sex-specific phenotype seen in C and D. (**F, G**) Growth curves as in Figure 5D and 5E, but comparing the mutants with a paternal transmission of the deletion with their WT littermates. The paternal deletion behaves as a silent mutation with no growth-related phenotype in the progenies. n=10–25 mice were analyzed per genotype, depending on age and sex. (**H**) Bisulfite-pyrosequencing shows an almost complete rescue of the *Zdbf2*-LOF defects of sDMR methylation in tissues of *Zdbf2*-GOF /*Zdbf2*-LOF mice at 6 weeks. Data are shown as means ± s.e.m. from n individuals. Statistical analyses were performed by a two-tailed, unpaired, nonparametric Mann Whitney t test. *p ≤ 0.05

Glaser et al._ Supplemental Figure 6

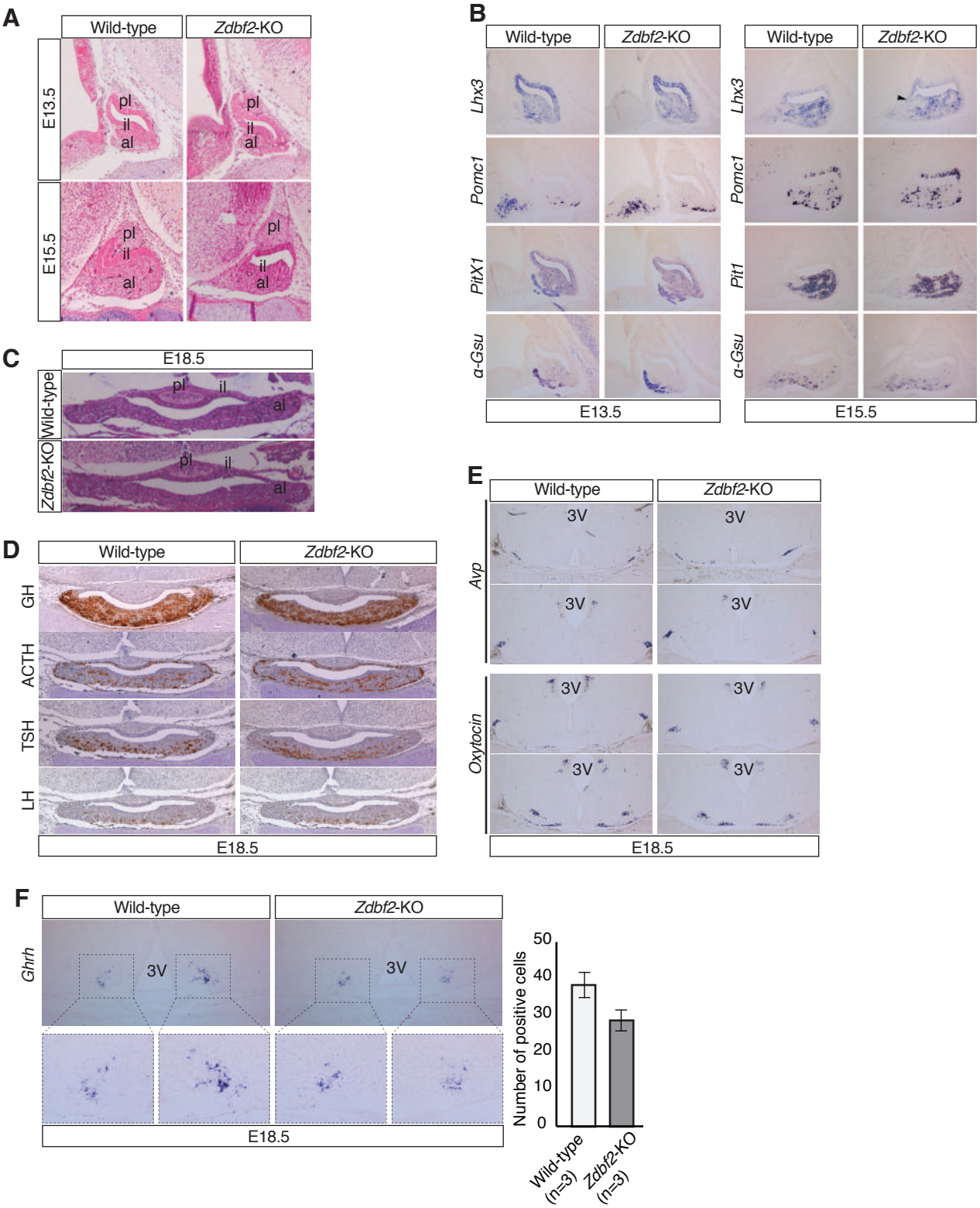

<u>Figure S6</u>: Normal development of the hypothalamo-pituitary axis in *Zdbf2*-KO mice.
(**A**) Haematoxylin-Eosin (H&E) staining reveals normal development of the pituitary at embryonic day (E) 13.5 and E15.5 embryonic days. (**B**) RNA in situ hybridization for pituitary lineage-specific genes reveals normal mRNA expression of cell specification markers in the pituitary of the *Zdbf2*-KO embryos at E13.5 and E15.5. (**C**) Morphological assessment of the mature E18.5 pituitary gland by H&E staining shows no phenotype in the pituitary gland before birth. (**D**) Immunohistochemistry analysis of four pituitary hormones (GH, ACTH, TSL, LH) at E18.5 suggests no obvious defect in hormone-producing cells in the anterior lobe of the pituitary before birth. (**E**) In situ hybridization for two hypothalamic neuropeptides, arginine vasopressin (AVP) (top) and oxytocin (bottom), in the developing E18.5 hypothalamus suggests no apparent differences in AVP and oxytocin transcripts. (**F**) RNA in situ hybridization for *Ghrh* on E18.5 hypothalamus shows trend towards decreased expression of *Ghrh* in mutant embryos compared to controls, although difference is not statistical significant. Quantification (right panel) represents the means ± s.e.m of the number of *Ghrh* positive cells over n=3 independent experiments. Overall, results in **A-F** are congruent with the observation of normal weight distribution in *Zdbf2*-KO E18.5 embryos (Figure 2B). pl, posterior lobe; il, intermediate lobe; al, anterior lobe; 3V, third ventricle of the hypothalamus.

Glaser et al._ Supplemental Figure 7

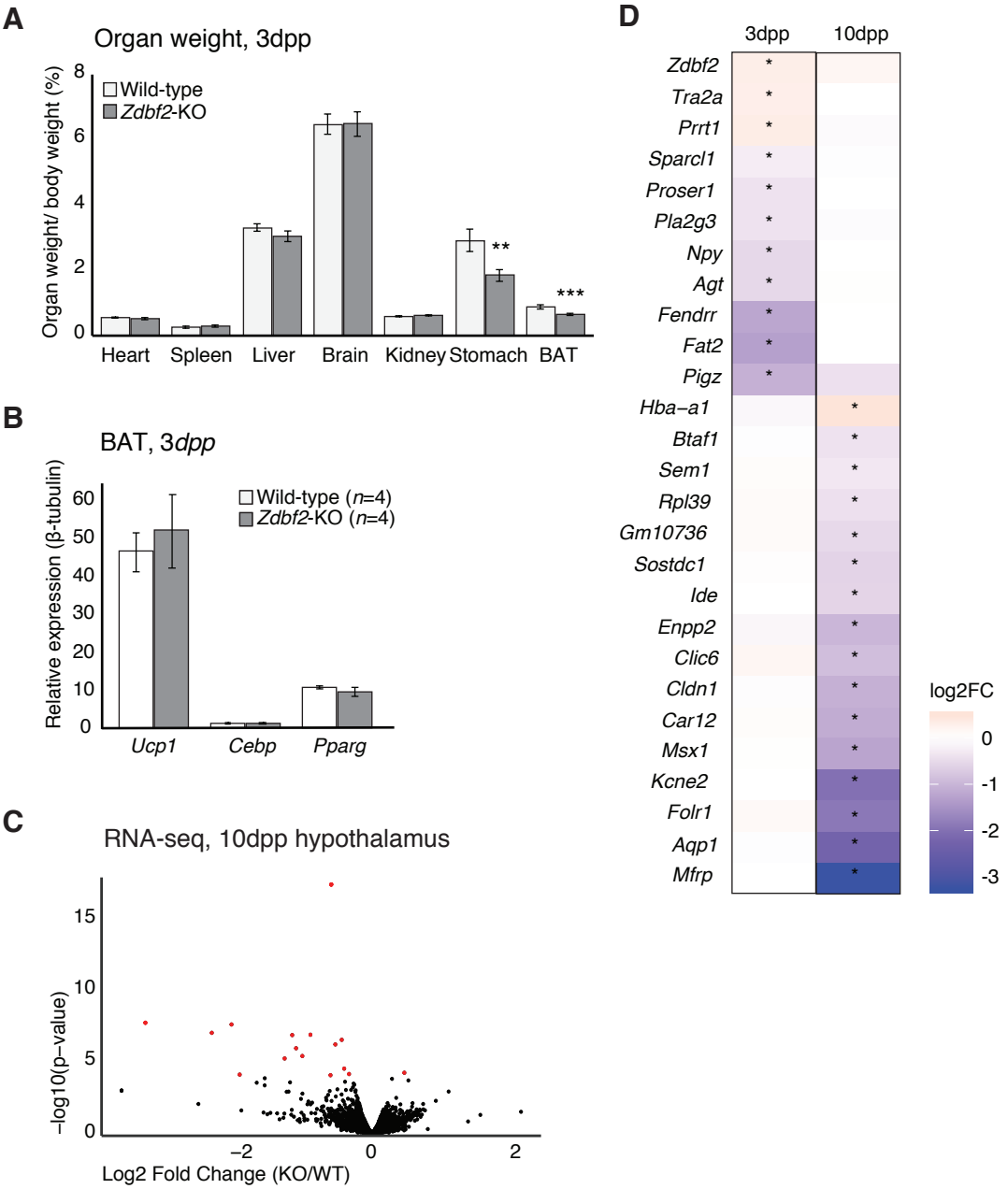

<u>Figure S7</u>: Characterization of the early postnatal feeding behavior in *Zdbf2*-KO pups. (**A**) Individual organ weight plotted as percentage of total body weight in *Zdbf2*-KO mice and WT littermates at 3dpp. (**B**) RT-qPCR from BAT measuring the mRNAs level of three markers of BAT activity (*Ucp-1*, *Cebp* and *Pparg*) between WT and *Zdbf2*-KO at 3dpp. (**C**) Volcano plot representation of RNA-seq of 10dpp hypothalamus of *Zdbf2*-KO versus WT littermates. Red dots: differentially expressed genes with a threshold of FDR<10%. (**D**) Heatmap showing the log2 fold change of expression of the differentially expressed genes (DEGs) in the hypothalamus of *Zdbf2*-KO pups at 3 and 10dpp. There is no overlap between the DEGs at 3 and 10dpp. Stars represent significant change of expression (FDR<10%).

<u>Supplemental Table 1</u>: Survivability counts from different transmission of the *Zdbf2*-KO allele.

***A. Zdbf2*-KO (paternal transmissiom)**																					
Days post partum		1	3	5	7	9	11	13	15	17	19	21	28	35	42	49	56	63	70	77	84
n=24 litters	Males WT	44	37	37	37	37	37	37	37	37	36	36	36	36	36	36	36	36	36	36	36
	Female WT	50	44	44	44	44	44	44	44	43	43	40	39	39	39	39	39	39	39	39	39
	Males KO	30	17	17	17	17	16	16	16	16	16	16	16	16	16	16	16	16	16	16	16
	Female KO	57	30	30	30	30	29	29	29	28	28	28	28	28	28	28	28	27	27	27	27

***B. Zdbf2*-KO (homozygote transmissiom)**																						
Days post partum		1	2	3	4	5	6	7	8	9	10	11	12	13	14	15	16	17	18	19	20	21
n=19 litters	Males KO	71	54	54	54	54	54	54	54	54	54	54	53	53	53	53	53	53	53	53	52	52
	Female KO	80	62	58	58	58	58	58	58	58	58	58	58	58	58	58	58	58	58	58	57	57

***C. Zdbf2*-Δexon6 (maternal transmissiom)**														
Days post partum		1	7	14	21	28	35	42	49	56	63	70	77	84
n=11 litters	Males WT	19	16	15	15	15	15	15	15	15	15	15	15	15
	Female WT	19	14	14	14	14	14	14	14	14	14	14	14	14
	Males KO	16	14	14	14	14	13	13	13	13	13	13	13	13
	Female KO	31	24	24	24	24	24	24	24	24	24	24	24	24

<u>Supplemental Table 1</u>: Survivability counts from different transmission of the *Zdbf2*-KO allele.

(A) Number of living pups followed every two days from 1 to 21dpp and every week from 21 to 84dpp from 24 litters coming from [female WT x male *Zdbf2* KO/WT] crosses (paternal transmission). These 24 litters come from 4 different crosses including 8 females and 4 males. Day 1 corresponds to the day of birth (1dpp). We can observe that the number of living *Zdbf2*-KO (males and females) starts decreasing from 3dpp onwards.

(B) Number of living pups followed every day from 1 to 21dpp from 19 litters coming from [female WT x male *Zdbf2* KO/KO] crosses (homozygote transmission). These 19 litters come from 5 different crosses including 10 females and 5 males. All pups from these crosses inherited a mutated allele from their dad and are thus *Zdbf2*-KO.

(C) Number of living pups followed every week from 1 to 84dpp from 11 litters coming from [female *Zdbf2* KO/WT x male WT] crosses (maternal transmission, silent mutation). These 11 litters come from 2 different crosses including 4 females and 2 males. We did not observe any survivability bias within those litters.

Supplemental Table 2: List of primers used in this study.

RT-qPCR primer		
Zdbf2 exons 1-3	Fwd	CCGGAAGGAGAGCAGGAG
	Rev	GAGCAGAAAAGAGCAAGCA
Zdbf2 exons 6-7	Fwd	CTGCGACACCACCCATATAA
	Rev	AAAACCACCACCACTTCAGG
Rplp0	Fwd	TCCAGAGGCACCATTGAAATT
	Rev	TCGCTGGCTCCCACCTT
Rrm2	Fwd	CCGAGCTGGAAAGTAAAGCG
	Rev	ATGGGAAAGACAACGAAGCG
Gh exons 4-5	Fwd	CTTGAGGATCTGCCCAACAC
	Rev	CCTCGGACCGTGTCTATGAG
Igf-1 exons 2-3	Fwd	TGGATGCTCTTCAGTTCGTG
	Rev	CACTCATCCACAATGCCTGT
18S	Fwd	GCCCTGTAATTGGAATGAGTCCACTT
	Rev	GTCCCCAAGATCCAACTACGAGCTTT
ßActin	Fwd	AAGTGACGTTGACATCCG
	Rev	GATCCACATCTGCTGGAAGG

RT-pyrosequencing		
Zdbf2 exon 6	Fwd	[Biotin]-GGAAATGAAGAGCAGCCCAGTAG
	Rev	GCCACTGTCTCAAGAGAACCATCA
	Seq	AACCATCACGTTCAGG

Bisulfite + Pyrosequencing Primers		
sDMR	Fwd	AGATGGAAGGAAAGAATTGAATTTTATA
	Rev	[Biotin]-TACCAACCCACTATATACATTCTTCATTA
	Seq	TGAATTTTATATATTATTTTTTGAT

Bisulfite + Cloning/Sequencing Primers		
sDMR	Outer Fwd	ATTTTATGTATTTATTAGTGAGTTG
	Outer Rev	CTAATCACAACTCCCAATCAC
	Inner Fwd	GAATTGAATTTTATATATTATTTTTTG
	Inner Rev	CCTATATACAACTTACCTTACTT

Genotyping Primers		
Zdbf2-KO	Fwd	AGCACATTTTCTTCCATTTACTTGT
	Rev	ACTCCAGTACCCCACACACA
Zdbf2-GOF	Fwd	CACCGATTGCTAGAACTACAATGG
	Rev	GAAAGCAATGCACACACTGG
Liz-LOF	Fwd	TTTTTCTTTTGCCTCCAAGAA
	Rev	CCTGGACAGCATTTCTTTCTC
	Rev	TGGCTTTAAAACAGGGGATG

CRISPR sgRNA oligos		
Zdbf2-KO	Left	CACCGCATTACAATGTATGCTACGA
		AAACTCGTAGCATACATTGTAATGC
	Right	CACCGTTTACCATGGATGCACTCCC
		AAACGGGAGTGCATCCATGGTAAAC